

1 **Exosome component 1 cleaves single-stranded DNA and sensitizes kidney renal**  
2 **clear cell carcinoma cells to poly(ADP-ribose) polymerase inhibitor**

3 Qi Xiao<sup>1,†</sup>, Qiaoling Liu<sup>1,†</sup>, Lina Wang<sup>1</sup>, Na Wang<sup>1</sup>, Kai Wang<sup>1</sup>, Chengli Song<sup>1,\*</sup> and  
4 Qingkai Yang<sup>1,\*</sup>

5

6 <sup>1</sup>Institute of Cancer Stem Cell, DaLian Medical University, 9 Western Lvshun South  
7 Road, Dalian, Liaoning 116044, China.

8

9 †These authors contributed equally to this work.

10

11 \*For correspondence: Yangqingkai@dmu.edu.cn; Chenglisong2015@hotmail.com.

12

13 **Abstract**

14 Targeting DNA repair pathway offers an important therapeutic strategy for cancers.  
15 However, the failure of DNA repair inhibitors to markedly benefit patients  
16 necessitates the development of new strategies. Here, we show that exosome  
17 component 1 (EXOSC1) promotes DNA damages and sensitizes kidney renal clear  
18 cell carcinoma (KIRC) cells to DNA repair inhibitor. Considering that endogenous  
19 source of mutation (ESM) constantly assaults genomic DNA and likely sensitize  
20 cancer cells to the inhibitor, we first analyzed the statistical relationship between the  
21 expression of individual genes and the mutations for KIRC. Among the candidates,  
22 EXOSC1 most notably promoted DNA damages and subsequent mutations via  
23 preferentially cleaving C site(s) in single-stranded DNA. Consistently, EXOSC1 was  
24 more significantly correlated with C>A transversions in coding strands than these in  
25 template strands in KIRC. Notably, KIRC patients with high EXOSC1 showed a poor  
26 prognosis, and EXOSC1 sensitized cancer cells to poly(ADP-ribose) polymerase  
27 inhibitor. These results show that EXOSC1 acts as an ESM in KIRC, and targeting  
28 EXOSC1 might be a potential therapeutic strategy.

29

30

31

32

33

## 34 **Introduction**

35 DNA damages and subsequent mutations are central to development, progression,  
36 and treatment of nearly all cancers (Brown et al., 2017; Farmer et al., 2005; Jeggo et  
37 al., 2016; Pearl et al., 2015; Roos et al., 2016). Cancer cells frequently decreases DNA  
38 repair pathways and increases endogenous sources of mutation (ESM) to drive  
39 mutations (Brown et al., 2017; Farmer et al., 2005; Jeggo et al., 2016; Pearl et al.,  
40 2015; Roos et al., 2016). Hence, cancer cells are often more reliant on a subset of  
41 DNA repair pathway(s) to survive DNA damages. While, targeting critical DNA  
42 repair members, such as poly (ADP-ribose) polymerases (PARPs) (Brown et al., 2017;  
43 Tubbs and Nussenzweig, 2017), offers a therapeutic strategy for cancers (Tutt et al.,  
44 2010). Inhibition of PARPs by small-molecule compounds disrupts the ability of  
45 cancer cells to survive ongoing DNA damage and results in cell cycle arrest and/or  
46 cell death (Lord and Ashworth, 2012). However, failure of PARP inhibitors (PARPis)  
47 to markedly benefit patients suggests the necessity for developing new strategies. Due  
48 to the central role of ESM in ongoing DNA damages, there is a need for the  
49 identification and understanding of ESM.

50 ESM constantly assaults genomic DNA and almost inevitably leads to mutations  
51 (Figure 1A) (Jeggo et al., 2015; Roos et al., 2015). However, most of ESM studies  
52 were focused on the deamination. The significance of deamination as an ESM is  
53 supported mainly by two observations: (1) Transitions show higher frequency than  
54 expected by chance, although there are twice as many possible transversions.  
55 Nucleotide substitutions consist of two types: transition and transversion (Alexandrov  
56 et al., 2013a; Burgess, 2019; Petljak et al., 2019). Transition is a substitution in which  
57 one base is replaced by another of the same class (purine or pyrimidine), while  
58 transversion is a substitution in which a purine is replaced with a pyrimidine or vice  
59 versa (Figure 1B). (2) C>T transitions at methylated cytosine in CG base pairs display  
60 a higher frequency than expected (Alexandrov et al., 2013a; Alexandrov et al., 2013b;  
61 Burgess, 2019; Hutchinson, 2013; Petljak et al., 2019). Therefore, activation-induced  
62 cytidine deaminase (AID) (Barlow et al., 2013; Greaves, 2018; Petersen-Mahrt et al.,  
63 2002) and apolipoprotein B mRNA editing enzyme catalytic (APOBEC) family  
64 (Alexandrov et al., 2013b; Buisson et al., 2019; Hutchinson, 2013; McGranahan et al.,  
65 2017; Robertson et al., 2017) catalyzing the deamination of C were identified as  
66 ESMs. Unfortunately, some cancers such as kidney renal clear cell carcinoma (KIRC)  
67 show the low mutation proportion at CG base pairs and low APOBEC expression

68 (Burns et al., 2013b), raising the potential roles of unidentified ESMs.

69 Due to advances in sequencing technology and the great efforts of The Cancer  
70 Genome Atlas (TCGA), it is now possible to explore the statistical relationship  
71 between mutations and the expression of individual genes in multiple cancer types  
72 (Weinstein et al., 2013). The majority of patients included in the TCGA database are  
73 accompanied by data regarding both mutations and genome-wide expression of  
74 individual genes (Weinstein et al., 2013). Because that DNA damages often comprise  
75 a major source of mutation, the relativity between DNA damage and mutation allows  
76 quantitative analyses of mutation to be taken as a proxy of DNA damage (Brown et al.,  
77 2017; Jeggo et al., 2016; Pearl et al., 2015). Furthermore, the gene-specific correlation  
78 between mRNA and protein levels allows quantitative analyses of individual gene  
79 expression as an indicator for the corresponding protein (Peng et al., 2015; Uhlen et  
80 al., 2017; Zhang et al., 2017). Hence, analyses of the cancer cohort may identify  
81 candidate ESMs (Tubbs and Nussenzweig, 2017).

82 The exosome is an evolutionarily conserved multiprotein complex formed by  
83 exosome components (EXOSCs) (Bousquet-Antonelli et al., 2000; Brown et al., 2000;  
84 Tomecki et al., 2010). In eukaryotes, the exosome complex has a “ring complex”  
85 (EXOSC4–EXOSC9) and a “cap” structure (EXOSC1–EXOSC3) (Figure 1C). The  
86 human exosome complex may also contain two additional subunits, EXOSC10 and  
87 EXOSC11 (Jonathan et al., 2006; Lorentzen et al., 2008; Quansheng et al., 2006;  
88 Wasmuth et al., 2014), which provide 3' to 5' exo- and/or endoribonuclease activities  
89 (Januszyk and Lima, 2014; Kilchert et al., 2016). The exosome is well known to  
90 degrade RNA (Januszyk and Lima, 2014; Kilchert et al., 2016; Ulmke et al., 2021).  
91 Hence, the exosome was reported to protect cells from genomic instability via  
92 degrading the DNA/RNA hybrids and restricting DNA strand mutational asymmetry  
93 (Lim et al., 2017; Pefanis and Basu, 2015; Pefanis et al., 2015). Interestingly, the cap  
94 unit EXOSC2 stably associated with the exosome complex, while EXOSC1 is not  
95 stably associated (Dai et al., 2018; Malet et al., 2010), suggesting that EXOSC1 might  
96 be involved in some functions independent of the complex.

97 In this study, we show that EXOSC1 acts as an ESM and sensitizes cancer cells to  
98 PARPi in KIRC. Due to the role of exosome in maintaining genomic stability, these  
99 results also indicate that a unit of multiprotein complex can play a role opposite to  
100 that of the complex.

101

## 102 **Results**

### 103 **Identification of candidate ESMs in KIRC**

104 Because that ESMs constantly assaults genomic DNA, we hypothesized that ESMs  
105 likely sensitized cancer cells to the inhibitors of DNA repair pathways. Considering  
106 that substitution is the most abundant mutation in all cancers, we initiated this study to  
107 identify candidate ESMs responsible for substitution mutations. To identify the  
108 candidate ESMs other than deamination, we focused on KIRC for three reasons: (1)  
109 KIRC shows the lowest proportion of mutations at CG in major cancer types (Burns  
110 et al., 2013b), suggesting that the deamination contributes less to the mutations in  
111 KIRC. (2) only low expressions of AID and APOBECs were detected in KIRC (Burns  
112 et al., 2013b). (3) The kidney potentially suffers less from exogenous source of  
113 mutations (EOSMs) (Loeb, 2011; Roberts and Gordenin, 2014). RNA-seq and exomic  
114 mutation data corresponding to 532 KIRC patients and 30,254 somatic substitution  
115 mutations in the TCGA were retrieved from The cBio Cancer Genomics Portal  
116 (<http://cbioportal.org>) (Figure 1D). Because that ESMs likely show similar impact on  
117 the template and code DNA strands, the 12 types of substitution were groups into 6  
118 types of complementary substitution (c-substitution) to simplify the analyses (Figure  
119 1D).

120 Spearman's rank analysis was first performed to assess the correlation between  
121 each c-substitution type and the genome-wide expression of individual genes.  
122 Resultant  $p$  and  $r$  values were used for the further analyses. For example, GAPDH  
123 showed a  $p = 0.0011$  and  $r = 0.16$  correlation with C>A/G>T c-substitution, indicating  
124 that GAPDH expression displayed a positive correlation with C>A/G>T (Figure 1E).  
125 Similarly, CRB3 ( $p = 0.0003$ ,  $r = 0.17$ ) was positively correlated with A>T/T>A  
126 (Figure 1E). Although the  $p$  values of multiple genes were lower than 0.05 (Figure  
127 1F), only top ranked 200 genes (approximately 1% of the genome-wide genes) were  
128 taken as the candidates for each c-substitution type (Supplementary Table S1).

129 Student's  $t$ -test analysis was then used to determine whether the expression  
130 difference of individual gene between the high and low c-substitution groups is  
131 significant. The expression of individual genes in each patient was normalized by a  
132 house keeping gene, TATA-binding protein (TBP) as previously described (Burns et  
133 al., 2013a; Burns et al., 2013b). According to each c-substitution, 532 KIRC patients  
134 were groups into 3 groups (high, medium and low). The difference of individual gene  
135 between high and low c-substitution mutation groups was then analyzed by student's

136 *t*-test. Resultant *p* and fold of change (FC) values were used for the further analyses.  
137 For example, ASNS with  $p = 0.0005$  and  $FC = 1.39$ , indicating that ASNS was  
138 increased in the high group (Figure 1G). Although the *p* values of multiple genes were  
139 lower than 0.05 (Figure 1H), only top 200 genes with high FC and  $p < 0.05$  were  
140 taken as the candidates (Supplementary Table S2). Notably, none of APOBEC family  
141 members were identified as candidate by correlation or student's *t*-test analyses,  
142 supporting that deamination contributes less to the mutations in KIRC.

143 Next, we performed meta-analyses to determine which of the 6 c-substitution types  
144 to be focused on. Mutation frequencies of c-substitution types were first analyzed in  
145 five major cancers: breast adenocarcinoma (BRCA), glioblastoma multiforme (GBM),  
146 bladder urothelial carcinoma (BLCA), acute myeloid leukemia (AML) and KIRC,  
147 which potentially suffer less from the EOSMs. As shown in Figure 1I, KIRC  
148 displayed higher frequencies of C>A/G>T, A>T/T>A, and A>C/T>G mutations.  
149 Using tumor protein p53 (TP53) as control, we then assessed the frequencies of  
150 c-substitution types in von Hippel-Lindau tumor suppressor (VHL), the most  
151 frequently mutated gene in KIRC. Consistent with previous studies (Burns et al.,  
152 2013a; Kandoth et al., 2013), the most frequent c-substitution type of TP53 mutations  
153 in BRCA was C>T/G>A (Figure 1J), while the most frequent type of VHL mutations  
154 in KIRC was C>A/G>T ( $p = 0.004$ , chi-squared test) (Figure 1K). Even after  
155 normalization according to the base frequency, this phenomenon was still observed ( $p$   
156 = 0.021) (Figure 1—figure supplement 1A and B). Further Kaplan–Meier (KM)  
157 analysis of overall survival (OS) indicated that patients with VHL C>A/G>T  
158 mutations showed poor OS (Figure 1L). These observations raised the significance of  
159 C>A/G>T c-substitutions in KIRC.

160 We then evaluated the expression difference of individual gene between the VHL  
161 C>A/G>T mutation positive and negative patients. Student's *t*-tests analyses showed  
162 that 66 genes displayed  $p < 0.05$  (Supplementary Table S3). Further overlap analyses  
163 demonstrated that cyclin B1 (CCNB1), exosome component 1 (EXOSC1), and RAB5  
164 interacting factor (RAB5IF) were identified as candidate ESMs for C>A/G>T by all  
165 of the above analyses (Figure 1M).

166

### 167 **EXOSC1 promotes mutations in *E. coli***

168 To evaluate the capability of the candidate gene to promote mutation,  
169 rifampicin-resistant assay in *E. coli* was performed as previously described

170 (Petersen-Mahrt et al., 2002). Because that mutation of the rifampicin-targeted *rpoB*  
171 gene to rifampicin resistance ( $\text{Rif}^{\text{R}}$ ) occurs at a low frequency, the capability of a gene  
172 to mutate *rpoB* to  $\text{Rif}^{\text{R}}$  can be evaluated by fluctuation analysis (Petersen-Mahrt et al.,  
173 2002). AID, an known ESM (Petersen-Mahrt et al., 2002), was used as a positive  
174 control. Four genes (CDK5, TARBP2, PSAT1 and NECAB3) were used as random  
175 controls (Figure 2—figure supplement 1A and Supplementary Table S4). These genes  
176 were expressed in *E. coli* under the regulation of a *trp/lac* (*tac*) hybrid promoter,  
177 which could be activated by isopropyl  $\beta$ -D-1-thiogalactopyranoside (IPTG) (Figure  
178 2A). Consistent with a previous study (Petersen-Mahrt et al., 2002), AID enhanced  
179 mutation in *E. coli* (Figure 2B). Notably, EXOSC1 more significantly increased  
180 mutations than AID did ( $p = 4.08 \times 10^{-5}$ ) (Figure 2B). We then evaluated the  
181 capabilities of EXOSC1 homologs (EXOSC2–EXOSC9) to promote mutations  
182 (Figure 2—figure supplement 1B). Among the members of exosome complex,  
183 EXOSC1 most notably enhanced mutation in *E. coli* ( $p = 3.5 \times 10^{-11}$ ) (Figure 2C). To  
184 determine whether the increase in mutation frequency stemmed from EXOSC1  
185 protein itself, rifampicin-resistant assays were performed in the presence or absence  
186 of IPTG, the transcriptional inducer. As shown in Figure 2E–F, IPTG absence notably  
187 decreased the mutation frequency ( $p = 1.29 \times 10^{-9}$ ), indicating that the protein of  
188 EXOSC1 promoted the mutation. Additionally, we evaluated the impact of EXOSC1  
189 on the growth of *E. coli*. As shown in Figure 2—figure supplement 1C, EXOSC1  
190 expression only slightly decreased cell growth, which might be due to the increase in  
191 mutation burden (Schaaper and Dunn, 1987).

192 Next, the mutation spectra of  $\text{Rif}^{\text{R}}$  were analyzed by sequencing the *rpoB* gene  
193 PCR products from rifampicin-resistant clones. Sequencing of *rpoB* gene in 25  
194 randomly selected rifampicin-resistant clones indicated that most of mutations in  
195 control clones were C>T/G>A transitions, while EXOSC1 frequently promoted  
196 C>A/G>T transversion mutations (Figure 2G–I). Moreover, most of C>A/G>T  
197 transversions in EXOSC1-transformed cells were clustered at C1576 (10/36 mutations)  
198 and C1699 (6/36 mutations), whereas C>T/G>A transitions in control cells showed a  
199 distinct distribution with major hot spots at C1565 (6/32 mutations) and C1721 (5/32  
200 mutations) (Figure 2G). Hence, it was suggested that the mutations in control and  
201 EXOSC1-transformed cells were promoted by distinct mechanism. Interestingly,  
202 EXOSC1-transformed cells also showed a shift of C>A/G>T mutations from 6%  
203 (2/32 mutations) to 69% (25/36 mutations) ( $p = 4.03 \times 10^{-7}$ , chi-squared test) (Figure

204 2H–J). Even after normalization to the base frequency, this phenomenon was still  
205 significant ( $p = 1.47 \times 10^{-6}$ ) (Figure 2—figure supplement 1D).

206

### 207 **EXOSC1 cleaves single-stranded DNA**

208 Considering that the exosome is well known to degrade RNA, we speculated that  
209 EXOSC1 might promote mutation through cleaving DNA. EXOSC1 was expressed  
210 and purified *in vitro* (Figure 3A). The resultant EXOSC1 protein was incubated with  
211 generic single-stranded DNA (ssDNA), double-stranded DNA (dsDNA) or the hybrid  
212 of DNA-RNA (Figure 3B). Polyacrylamide TBE-urea gel analyses of the resultant  
213 mixtures indicated that EXOSC1 notably cleaved ssDNA, while it displayed no  
214 detectable capability to cleave dsDNA or DNA-RNA hybrid (Figure 3C).

215 We then evaluated the capabilities of EXOSC1 homologs (EXOSC2–EXOSC9) to  
216 cleave ssDNA. The EXOSC protein was separately incubated with ssDNA. Gel  
217 analyses of the resultant mixtures indicated that, unlike EXOSC1, none of  
218 EXOSC2–EXOSC9 detectably cleaved ssDNA (Figure 3—figure supplement 1A).  
219 Considering that EXOSC1 is well known to form a complex with other exosome  
220 members, we also assessed the impact of the exosome members on the cleavage  
221 activity of EXOSC1. EXOSC1 was incubated with ssDNA in the presence of  
222 individual EXOSC1 homolog. Interestingly, EXOSC6, EXOSC7 and EXOSC8  
223 decreased EXOSC1 cleavage activity (Figure 3D), while EXOSC2, EXOSC3,  
224 EXOSC4 and EXOSC9 showed no detectable impact (Figure 3—figure supplement  
225 1B). We then evaluated the impact of the reaction components and pH on the cleavage  
226 activity of EXOSC1. It was found that  $K^+$  and  $Mg^{2+}$  enhanced the cleavage activity of  
227 EXOSC1 (Figure 3E), and EXOSC1 showed the highest cleavage activity at pH 7.0  
228 (Figure 3F). Further analyses indicated that the cleavage rate of EXOSC1 was  
229 approximately  $4 \times 10^{-4}$ /min at 37 °C (Figure 3G and H).

230

### 231 **EXOSC1 prefers to cleave C sites in single-stranded DNA**

232 Considering that conserved exosome prefers to degrade the RNA with specific  
233 sequence (Cvetkovic et al., 2017), we determined whether EXOSC1 preferred to  
234 cleave some site(s) in ssDNA. EXOSC1 was incubated with DNAs containing  
235 unbiased sequence and distinct 3' end. Consistent with the result of the generic DNA,  
236 EXOSC1 cleaved unbiased ssDNA and displayed no detectable capability to cleave  
237 dsDNA or DNA-RNA hybrid (Figure 4A and Figure 4—figure supplement 1A). And

238 only EXOSC1 displayed cleavage activity against unbiased ssDNA (Figure 4B).  
239 Interestingly, the cleavage rate against unbiased ssDNA (approximately  $1.2 \times$   
240  $10^{-3}/\text{min}$ ) was higher than that against generic ssDNA (Figure 4—figure supplement  
241 1B), suggesting that the DNA sequence might show some impact on the activity of  
242 EXOSC1. Notably, mass spectrometry (MS) analyses demonstrated that the resultant  
243 mixtures contained more free C than the other three base types (Figure 4E),  
244 suggesting that EXOSC1 preferred to cleave C sites in ssDNA. Since EXOSC1 was  
245 correlated with the C>A/G>T c-substitution type, it was likely that EXOSC1 cleaved  
246 C sites in ssDNA and subsequently resulted in C>A mutations through “A” rule DNA  
247 repair.

248 To evaluate the above hypothesis, we then determined whether EXOSC1-promoted  
249 mutations displayed strand asymmetries. Considering that EXOSC1 cleaved C sites in  
250 ssDNA but not DNA-RNA hybrid, we speculated that “transcribed” temple strands  
251 likely bound by RNA were less cleaved by EXOSC1. As shown in Figure 4F, C>A  
252 transversions in the “untranscribed” coding strand lead to C>A mutations in a gene,  
253 while C>A transversions in the “transcribed” template strand result in G>T mutations.  
254 Therefore, the capability of EXOSC1 to promote strand mutational asymmetry can be  
255 evaluated by comparing C>A and G>T frequencies. We first analyzed the  
256 distributions of C>A and G>T substitutions, instead of the distributions of C>A/G>T  
257 c-substitution, in the EXOSC1-transformed *E. coli* cells described above. As shown in  
258 Figure 4—figure supplement 1E and F, C>A substitution in *rpoB* gene were generated  
259 at a much higher frequency than G>T. Compared with the control, EXOSC1 enhanced  
260 C>A from 0% to 69% ( $p = 2.67 \times 10^{-7}$ ), while EXOSC1 only enhanced G>T from 6%  
261 to 17% even without a significance ( $p = 0.27$ ) (Figure 4—figure supplement 1E and  
262 F). Next, we evaluated C>A strand asymmetry in KIRC using spearman’s rank and  
263 student’s *t*-test analyses. Spearman’s rank analyses indicated that EXOSC1 showed  
264 the highest correlation (*r*) with C>A, and the correlation between EXOSC1 and G>T  
265 was even lower than that between EXOSC1 and C>A/G>T (Figure 4G and Figure  
266 4—figure supplement 1G). To evaluate the impact of group number on the further  
267 student’s *t*-test analyses, the KIRC patients were grouped into 2, 3, 4 or 5 groups  
268 according to the mutation types C>A, G>T, C>A/G>T and total (12 substitution  
269 types). As expected, the EXOSC1 differences between the low and high C>A/G>T  
270 groups were more significant than those between the low and high groups of total (12  
271 substitution types) mutations (Figure 4—figure supplement 1H and I). Importantly,



272 EXOSC1 showed more significant expression differences between the low and high  
273 C>A groups than those between the low and high G>T groups (Figure 4H and Figure  
274 4—figure supplement 1J), suggesting that EXOSC1 prefers to cleave C sites in  
275 ssDNA *in vivo*.

276

### 277 **EXOSC1 enhances DNA damage and mutations in KIRC cells**

278 Considering that EXOSC1 cleaves DNA *in vitro*, we then evaluated the capability of  
279 EXOSC1 to promote intracellular DNA damage using  $\gamma$ -H2AX staining and neutral  
280 comet tail assays. The 769-P and TUHR14TKB KIRC cells were transfected with the  
281 plasmid encoding EXOSC1 using empty vector as a control (Figure 5—figure  
282 supplement 1A).  $\gamma$ -H2AX staining analyses of the resultant cells demonstrated that  
283 EXOSC1 increased the  $\gamma$ -H2AX foci in the cells (Figure 5A). The number of  
284  $\gamma$ -H2AX-positive cells was increased approximately 7-fold by EXOSC1 (Figure 5B).  
285 While knockdown of EXOSC1 reduced the  $\gamma$ -H2AX foci (Figure 5C, and Figure  
286 5—figure supplement 1B and C). Consistent with the results of  $\gamma$ -H2AX staining,  
287 comet tail analyses also indicated that EXOSC1 increased DNA damage (Figure 5D  
288 and E).

289 Due to the central role of DNA damage in mutations, we performed differential  
290 DNA denaturation PCR (3D-PCR) to determine whether EXOSC1 enhances mutation  
291 in KIRC cells. Because that DNA sequences with more A/T content can be amplified  
292 at lower denaturation temperatures than parental sequences, 3D-PCR enables  
293 qualitative estimates of genomic C/G>A/T mutations in a population of cells. As  
294 shown in Figure 5F, the enhanced expression of EXOSC1 (EXOSC1-OE) increased  
295 lower temperature amplicons (LTAs) of VHL, suggesting that EXOSC1 increased the  
296 mutations in VHL gene. Consistently, further sequencing analyses of the LTAs  
297 indicated that EXOSC1-OE cells showed more C>A mutations in VHL gene (Figure  
298 5F).

299 Considering that the “A” rule DNA repair is dependent on X-ray repair  
300 cross-complementing 1 (XRCC1) (Sale et al., 2001), we knocked down XRCC1 to  
301 evaluate the role of XRCC1 in EXOSC1-promoted mutations (Figure 5—figure  
302 supplement 1D–F). 3D-PCR analyses of the resultant cells indicated that knockdown  
303 of XRCC1 impaired the capability of EXOSC1 to increase the LTAs (Figure 5G).  
304 Furthermore, both XRCC1 knockdown (XRCC1-KD) and EXOSC1 knockdown  
305 (EXOSC1-KD) decreased the LTAs (Figure 5H and I). Additionally, a subcutaneous

306 xenograft tumor model was used to determine whether EXOSC1 enhances DNA  
307 mutations *in vivo* (Figure 5J). Stable control (vector), EXOSC1-OE and EXOSC1-KD  
308 769-P cells were subcutaneously implanted. After two weeks, 3D-PCR analyses of the  
309 resultant tumors indicated that EXOSC1 increased the LTAs of VHL, whereas  
310 knockdown of EXOSC1 reduced the LTAs (Figure 5K), suggesting that EXOSC1  
311 enhanced mutations in KIRC.

312

### 313 **EXOSC1 sensitizes KIRC cells to PARP inhibitor**

314 Considering the central roles of mutation in the process of cancers, we evaluated the  
315 potential clinical significance of EXOSC1 in KIRC using KM analyses. KM analyses  
316 of disease-free survival (DFS) and OS were performed using the clinical data from  
317 532 KIRC patients in TCGA. The fragments per kilo base per million mapped reads  
318 (FPKM) were used to evaluate the expression of EXOSC1 in KIRC (Figure  
319 6—figure supplement 1A). The median-separation KM analyses indicated that high  
320 EXOSC1 group showed poor DFS and OS (Figure 6A and B). The median DFS in the  
321 low EXOSC1 group was 32.0-month longer than that in the high group ( $p = 9.78 \times$   
322  $10^{-8}$ , log-rank test) (Figure 6A). Consistently, the median OS in the low EXOSC1  
323 group was 36.9-month longer than that in high group ( $p = 2.2 \times 10^{-8}$ ) (Figure 6B). As  
324 expected, the best-separation KM analysis also indicated that high EXOSC1 group  
325 significantly showed poor OS ( $p = 2.6 \times 10^{-12}$ ) (Figure 6—figure supplement 1B).  
326 Due to the critical role of VHL mutation in KIRC, we then evaluated the potential  
327 clinical significance of EXOSC1 in the presence and absence of VHL mutation. KM  
328 analyses indicated that high EXOSC1 group showed poor OS in both presence  
329 (median OS (high vs low group) = 65.2 vs 98.5 months,  $p = 0.015$ ) and absence  
330 (median OS (high vs low group) = 75.7 vs 104.5 months,  $p = 1.0 \times 10^{-5}$ ) of VHL  
331 mutation (Figure 6C and Figure 6—figure supplement 1C).

332 Considering that EXOSC1 increases DNA damage, we speculated that EXOSC1  
333 potentially sensitizes KIRC cells to the inhibitor of poly(ADP-ribose) polymerase  
334 (PARP), which treats cancers via blocking DNA repair. As previously described (Li et  
335 al., 2020), colony formation assays were performed to evaluate the role of EXOSC1  
336 in the response to a PARP inhibitor, niraparib. Stable control (vector) and enhanced  
337 EXOSC1 (EXOSC1-OE) KIRC cells were seeded and treated with serial dilutions of  
338 niraparib until colonies were notably formed. As shown in Fig 6D–F, niraparib more  
339 notably inhibited the 769-P and TUHR14TKB KIRC cells with enhanced EXOSC1,

340 suggesting that EXOSC1 sensitized the cells to the inhibitor. Consistent with the  
341 results in 769-P and TUHR14TKB cells, EXOSC1 also sensitized SNU-1272 and  
342 Caki-2 KIRC cells to the inhibitor (Figure 6—figure supplement 1D). Next, we  
343 determined whether EXOSC1 could sensitize KIRC cells to niraparib in xenograft  
344 mouse models. The control and EXOSC1-OE cells were subcutaneously injected.  
345 Resultant tumor-bearing mice were grouped and treated by vehicle or niraparib.  
346 Consistent with the *ex vivo* results, niraparib more notably inhibited the tumor with  
347 enhanced EXOSC1 (Figure 6G and I), indicating that EXOSC1 sensitized KIRC  
348 xenografts to the inhibitor. No significant weight loss was observed throughout the  
349 study, suggesting that the niraparib treatment was well tolerated (Figure 6H and J).

350

## 351 Discussion

352 The genomic integrity of human cells is constantly assaulted by ESMs. Although  
353 human cells possess multi DNA repair mechanisms to counteract these constant  
354 assaults, not all lesions are correctly repaired and almost inevitably result in mutations.  
355 The central roles of these acquired mutations in nearly all cancers (Jeggo et al., 2015;  
356 Roos et al., 2015) emphasize the identification and understanding of the ESMs. Here,  
357 we show that EXOSC1 cleaves ssDNA and acts as an ESM in KIRC. Consistent with  
358 the capability of EXOSC1 to promote DNA damage and mutations, KIRC patients  
359 with high EXOSC1 showed a poor prognosis, and EXOSC1 also sensitized cancer  
360 cells to the PARP inhibitor.

361 Our results show that a unit of multiprotein complex can play a role distinct from  
362 the function(s) of the complex. Biological processes frequently require fine control  
363 over the formation of a multiprotein complex in a particular region of the cell. The  
364 exosome complex is well known for its roles in RNA degradation (Januszyk and Lima,  
365 2014; Kilchert et al., 2016). However, the role of exosome complex members other  
366 than RNA binding and degradation remains elusive. Interestingly, EXOSC1 can  
367 disassociate from the exosome complex (Dai et al., 2018; Malet et al., 2010),  
368 suggesting that EXOSC1 might be involved in some functions independent of the  
369 exosome. Our study demonstrated that EXOSC1 acts as an ESM to promote  
370 mutagenesis. Conversely, previous studies have described that the exosome, as a  
371 multiprotein complex, protects cells from genomic instability by preventing the  
372 formation of DNA/RNA hybrids and restricting DNA strand mutational asymmetry  
373 (Lim et al., 2017; Pefanis and Basu, 2015; Pefanis et al., 2015). This phenomenon can

374 at least partially be explained by the finding that some exosome members (EXOSC7  
375 and EXOSC8) can block the activity of EXOSC1 to cleave DNA. Therefore, a single  
376 EXOSC1 protein can show different responses depending on the presence/absence of  
377 its interacting partners. Further studies are needed to better understand the roles of the  
378 individual exosome member.

379 The potential pathological significance of EXOSC1 is supported by its association  
380 with poor DFS and OS in KIRC. Due to the capability of EXOSC1 to cleave DNA  
381 and promote mutations, EXOSC1 might enhance mutations and consequently provide  
382 genetic fuel for cancer development, metastasis, and even therapy resistance.  
383 Therefore, EXOSC1 might represent not only a KIRC marker but also a target to  
384 decrease the rate of KIRC evolution and stabilize the targets of existing therapeutics.  
385 Furthermore, targeting DNA repair in cancers by inhibiting PARPs offers an  
386 important therapeutic strategy (Cleary et al., 2020). Unfortunately, the failure of  
387 PARP inhibitors to markedly benefit patients enforces the necessity for developing  
388 new strategies to improve their efficacy (Cleary et al., 2020; Dizon, 2017; Lord and  
389 Ashworth, 2017). Our study demonstrated that EXOSC1 sensitized KIRC cells to  
390 PARP inhibitor, suggesting inhibition of PARPs might be a penitential strategy to treat  
391 KIRC patients with high EXOSC1. We also noticed that KIRC patients with high  
392 EXOSC1 and VHL mutations showed the poorest OS. Considering the DNA cleavage  
393 activity of EXOSC1 and the role of VHL in stabilizing the genome (Thoma et al.,  
394 2009; Zhang et al., 2018), we speculate that patients with the VHL mutation and high  
395 EXOSC1 might show higher possibility to benefit from PARP inhibitor(s).

396 However, several limitations of this study should be noted. First, we observed a  
397 notable variation in terms of the correlation with a different c-substitution type for a  
398 given gene, implying the need for further studies. Second, although we showed that  
399 EXOSC1 could cleave ssDNA and act as an ESM, we did not directly identify the  
400 mechanism responsible for turning the DNA cleavages into mutations. The role of  
401 XRCC1 in EXOSC1-promoted mutations was only briefly evaluated. Hence, we  
402 cannot exclude the possibility that other proteins might contribute to this process.  
403 Third, because that DNA cleavage by EXOSC1 should be independent of the cancer  
404 type, we propose that EXOSC1 likely contributes to the mutations in the cancers other  
405 than KIRC. And more work is still needed. Despite these limitations, our results still  
406 indicate that EXOSC1 acts as an ESM in KIRC.

407

## 408 **Materials and methods**

### 409 **Sample preparation**

410 Samples of 532 KIRC patients from TCGA used for expression and mutation analyses  
411 were collected through The cBio Cancer Genomics Portal (<http://cbioportal.org>) as  
412 described in our previous studies (Li et al., 2020; Zhou et al., 2019).

413

### 414 **Cell culture**

415 All cell lines were obtained from the American Type Tissue Collection. The 769-P,  
416 SNU-1272 and Caki-2 cells were maintained in RPMI 1640 medium containing 10%  
417 heat-inactivated FBS, 100 U/ml penicillin and streptomycin at 37 °C under a  
418 humidified atmosphere of 5% CO<sub>2</sub>. TUHR14TKB cells were maintained in DMEM  
419 containing 10% heat-inactivated FBS, 100 U/ml penicillin and streptomycin at 37 °C  
420 under a humidified atmosphere of 5% CO<sub>2</sub>. Transfections were performed using  
421 lipofectamine 2000 (Thermo Fisher Scientific Inc., Waltham, MA, USA).

422

### 423 **Antibodies, reagents and plasmids**

424 Anti-Flag (Cat. number: F7425) and anti-His (Cat. number: SAB1306085) antibodies  
425 were from Sigma-Aldrich (St. Louis, MS, USA). Anti-phospho- $\gamma$ -H2AX (Ser139)  
426 (Cat. number: 05-636) and anti-XRCC1 (Cat. number: SAB1306085) were from  
427 Millipore (Billerica, MA, USA). Anti-EXOSC1 (Cat. number: EPR13526) was from  
428 Abcam (Cambridge, MA, USA). Niraparib (Cat. number: HY-10619) and rifampicin  
429 (Cat. number: R3501) were from MedChem Express and Sigma-Aldrich, respectively.

430 Full-length EXOSC1 was cloned into the *Xba* I and *Nhe* I sites of the lentivirus  
431 vector pCDH-CMV-MCS-EF1-Puro (System Biosciences, Mountain View, CA, USA)  
432 to construct pCDH-Flag EXOSC1. CCGAGTTCCTACAGACCTAAG and  
433 CGAGGAACTATCCGCAAAGAA sequences were cloned into pLKO.1 to construct  
434 the pLKO shEXOSC1-1 and pLKO shEXOSC1-2 plasmids, respectively. Similarly,  
435 CCAGTGCTCCAGGAAGATATA and CGATACGTACAGCCTTCAAT sequences  
436 were cloned into pMKO.1 to construct the pMKO shXRCC1-1 and pMKO  
437 shXRCC1-2 plasmids, respectively. According to the knockdown efficiency (Figure  
438 5—figure supplement 1), pLKO shEXOSC1-1 and pMKO.1 shXRCC1-1 with higher  
439 knockdown efficiencies were used to generate EXOSC1-KD and XRCC1-KD cells.  
440 AID (NM\_020661.4), CDK5 (NM\_004935.4), TARBP2 (NM\_134323.1), EXOSC1  
441 (NM\_016046.5), RAB5IF (NM\_018840.5), CCNB1 (NM\_031966.4), PSAT1

442 (NM\_058179.4), NECAB3 (NM\_031232.3), EXOSC2 (NM\_014285.7), EXOSC3  
443 (NM\_016042.4), EXOSC4 (NM\_019037.3), EXOSC5 (NM\_020158.4), EXOSC6  
444 (NM\_058219.3), EXOSC7 (NM\_015004.4), EXOSC8 (NM\_181503.3) and EXOSC9  
445 (NM\_005033) were amplified and cloned into the pET-28a(+) vector (Novogen  
446 Limited, Hornsby Westfield, NSW, Australia) to construct the pET-28a-Gene-6XHis *E.*  
447 *coli* expression plasmids. PCR primers for the amplification of above genes are  
448 described in Supplementary Table S5.

449

#### 450 **Immunoblotting and immunofluorescence**

451 Immunoblotting and immunofluorescence were carried out as described in our  
452 previous study (Song et al., 2018; Wang et al., 2020).

453

#### 454 **Rifampicin-resistant assay in *E. coli***

455 Rifampicin-resistant assays were carried out as described previously (Petersen-Mahrt  
456 et al., 2002). Briefly, rifampicin-resistant assays for each gene were performed using  
457 30 independent cultures grown overnight to saturation in rich medium supplemented  
458 with 50 mg/L kanamycin and 1 mM IPTG. Rif<sup>R</sup> mutants were selected on medium  
459 containing 50 mg/L rifampicin. Mutation frequencies were assessed by determining  
460 the median number of rifampicin-resistant clones per 10<sup>9</sup> viable plated cells. The  
461 mutation spectra of Rif<sup>R</sup> were analyzed by sequencing the amplified rpoB 627-bp  
462 PCR products using 5'-TTGGCGAAATGGCGGAAAACC-3' and  
463 5'-CACCGACGGATACCACCTGCTG-3' primers.

464

#### 465 **Expression and purification of EXOSC proteins**

466 Expression and purification of EXOSC proteins were carried out as described in our  
467 previous study (Wang et al., 2020). pET-28a-EXOSCs-6XHises encoding His-tagged  
468 EXOSCs were introduced into BL21 (DE3)-pLysS, which were grown in nutrient-rich  
469 medium with 32Y (containing 3.2% (w/v) yeast extract, 0.8% (w/v) peptone and  
470 0.58% (w/v) NaCl) in 10 mM Tris-HCl at 30°C and pH 7.4. Protein expression was  
471 induced with 0.4 mM IPTG at 20°C for 20 h after the cells reached an OD<sub>600</sub> of  
472 0.4~0.5. Induced BL21 (DE3)-pLysS host cells without any plasmid were used as a  
473 negative control. The resultant cells were harvested by centrifugation at 5000 g for 10  
474 min and washed twice with ice-cold PBS. The collected cells were resuspended in

475 PBS (1 g of wet weight cells per 10 mL of PBS) containing 1 mM MgCl<sub>2</sub>, 20 mM  
476 imidazole, 1 tablet/50 mL protease inhibitor cocktail, and 100 U/mL DNase.  
477 Resuspended cells were broken by an ultrasonic wave. Cell lysates were centrifuged  
478 at 20,000 g at 4°C for 30 min to remove unbroken cells and debris.

479 After pre-equilibration with 10 column volumes (CV) of binding buffer (PBS  
480 containing 10% (v/v) glycerol and 20 mM imidazole, pH 7.6), Ni sepharose 6 Fast  
481 flow (GE Healthcare, New York, NY, USA) was applied for the purification of  
482 EXOSCs. The resins were washed 5 times and eluted using elution buffer (binding  
483 buffer containing 300 mM imidazole). EXOSCs were concentrated using an Amicon  
484 Ultrafree centrifugal filter (Millipore Corporation, Billerica, MA, USA) and  
485 pre-equilibrated with 10 mM HEPES buffer (pH 7.4) containing 150 mM NaCl and  
486 10% glycerol. Size-exclusion chromatography (SEC) with a Superdex-200 HiLoad  
487 10/600 column (GE Healthcare, New York, NY, USA) was used to further purify  
488 EXOSCs. The purity of the fractions was analyzed by coomassie blue staining. The  
489 protein concentration was determined using a BCA assay according to the  
490 manufacturer's instructions (Pierce, Rockland, IL, USA).

491

#### 492 **Cleavage activity assay *in vitro***

493 The cleavage assays of EXOSCs were carried out in reaction buffer modified from a  
494 previous study (Quansheng et al., 2006). Briefly, 50 µL of reaction mixture containing  
495 1 µM oligonucleotides, 1 µM EXOSC protein, 70 mM KCl, 700 µM MgCl<sub>2</sub>, 1 mM  
496 DTT, and 20 mM Tris-HCl pH 7.0 was incubated at 37 °C for 4 h. The reaction was  
497 stopped by addition of 10 µM proteinase K at 58°C for 10 min and heating at 90°C for  
498 30 s. The resultant samples were then analyzed using 15% polyacrylamide TBE-urea  
499 gels.

500

#### 501 **LC-MS/MS analysis**

502 LC-MS/MS analyses of deoxyadenine (A), deoxythymidine (T), deoxyguanine (G)  
503 and deoxycytocine (C) were carried out as described in our previous studies (Song et  
504 al., 2018; Wang et al., 2020).

505

#### 506 **Generation of stable cell lines**

507 Stable cell lines were generated as described in our previous study (Song et al., 2018;

508 Wang et al., 2020). Briefly, the TUHR14TKB, SNU-1272, 769-P and Caki-2 cells  
509 were infected with pCDH-CMV-MCS-EF1-Puro (empty vector used as control),  
510 pCDH-Flag EXOSC1 (EXOSC1-OE), pLKO.1-scramble shRNA (empty vector used  
511 as control), pLKO shEXOSC1-1 (EXOSC1-KD) or pLKO shEXOSC1-2 lentiviral  
512 particles, which were generated following the manufacturer's protocol (System  
513 Biosciences, Mountain View, CA, USA). The resultant cells were selected with  
514 puromycin for 2 weeks. These stable cells were then infected with virus encoding  
515 pMKO.1, pMKO.1 shXRCC1-1 (XRCC1-KD) or pMKO.1 shXRCC1-2. The  
516 resultant cells were selected with hygromycin B for 2 weeks to generate stable  
517 XRCC1 knockdown cells. According to the knockdown efficiency (Figure 5—figure  
518 supplement 1), shEXOSC1-1 and shXRCC1-1 with higher knockdown efficiencies  
519 were used as EXOSC1-KD and XRCC1-KD in this study.

520

#### 521 **$\gamma$ -H2AX staining and neutral comet tail assays**

522  $\gamma$ -H2AX staining and neutral comet tail assays were performed as described  
523 previously (Li et al., 2020).

524

#### 525 **3D-PCR and sequencing**

526 3D-PCRs of VHL mutations were carried out as described previously (Burns et al.,  
527 2013a) using first (5'-GAGTACGGCCCTGAAGAAGA-3' and  
528 5'-TCAATCTCCCATCCGTTGAT-3') and nested  
529 (5'-TGCGCTAGGTGAACTCGC-3' and 5'-GCGGCAGCGTTGGGTAGG-3') PCR  
530 primers. PCR products were then analyzed by gel electrophoresis, cloned into  
531 pMD20-T vector, and sequenced.

532

#### 533 **Colony-forming assay**

534 The colony-forming assays were performed as described in our previous study (Li et  
535 al., 2020).

536

#### 537 **Subcutaneous xenograft tumor growth *in vivo***

538 The following animal-handling procedures were approved by the Animal Care and  
539 Use Committee of Dalian Medical University. Xenograft models were carried out as  
540 described in our previous studies (Li et al., 2020; Song et al., 2018; Yang et al., 2010).  
541 Briefly,  $2 \times 10^6$  stable control/EXOSC1-OE 769-P and Caki-2 cells were suspended



542 and injected subcutaneously into the flank of 6-week-old nude mice. After 7 days,  
543 these tumor-bearing mice were randomized into 4 groups (6 mice per group) and  
544 treated by oral gavage twice a day with vehicle or niraparib (4 mg/kg). The mice were  
545 observed daily and weighed once per week. Tumor size was measured using a caliper,  
546 and the tumor volume was calculated using the following formula:  $0.52 \times L \times W^2$ ,  
547 where L is the longest diameter and W is the shortest diameter. Mice were euthanized  
548 when the tumors reached 1500 mm<sup>3</sup> or showed necrosis.

549

### 550 **Statistical analyses**

551 *P* values were calculated by the two-tailed student's *t*-test, log-rank test, fisher's  
552 exact-test, chi-squared test, or spearman correlation analyses as noted. *P* values < 0.05  
553 were considered statistically significant.

554

### 555 **Availability**

556 All data associated with this study are available in the main text or the supplementary  
557 materials.

558

### 559 **Experimental replicates and reproducibility**

560 All data presented in this paper are representative of 2–4 independent experiments  
561 with comparable results.

562

### 563 **Acknowledgements**

564 We would like to thank Dr. Wei Cheng (ICSC Core Facility, Dalian  
565 MedicalUniversity) for her material and technical support.

566

### 567 **Funding**

568 This study was supported by grants from the National Natural Science Foundation of  
569 China (NSFC Nos. 81872310 to Q.Y., and 82073123 to C.S.) and China Postdoctoral  
570 Science Foundation (2020M680956 to L.W.).

571

### 572 **Authors' contributions**

573 Q.Y. and C.S. designed the experiments and wrote the paper. Q.X., Q.L. and L.W. performed  
574 most experiments. Q.X. and Q.L. carried out EXOSC protein extraction. C.S. and W.L.  
575 performed bioinformatics analyses. N.W. and K.W. maintained the cells and performed some

576 of the western blot analyses. Q.L. and L.W. carried out the  $\gamma$ -H2AX staining and comet  
577 assays.

578

### 579 **Conflict of interest**

580 The authors declare no competing interests.

581

### 582 **References**

583 Alexandrov, L.B., Nik-Zainal, S., Wedge, D.C., Aparicio, S.A., Behjati, S., Biankin,

584 A.V., Bignell, G.R., Bolli, N., Borg, A., Borresen-Dale, A.L., *et al.* (2013a).

585 Signatures of mutational processes in human cancer. *Nature* *500*, 415-421.

586 Alexandrov, L.B., Nik-Zainal, S., Wedge, D.C., Aparicio, S.A., Behjati, S., Biankin,

587 A.V., Bignell, G.R., Bolli, N., Borg, A., Borresen-Dale, A.L., *et al.* (2013b).

588 Signatures of mutational processes in human cancer. *Nature* *500*, 415-421.

589 Barlow, J.H., Faryabi, R.B., Callen, E., Wong, N., Malhowski, A., Chen, H.T.,

590 Gutierrez-Cruz, G., Sun, H.W., McKinnon, P., Wright, G., *et al.* (2013). Identification

591 of early replicating fragile sites that contribute to genome instability. *Cell* *152*,

592 620-632.

593 Bousquet-Antonelli, C., , Presutti, C., , and Tollervey, D., . (2000). Identification of a

594 regulated pathway for nuclear pre-mRNA turnover. *Cell* *102*, 765-775.

595 Brown, J.S., O'Carrigan, B., Jackson, S.P., and Yap, T.A. (2017). Targeting DNA

596 Repair in Cancer: Beyond PARP Inhibitors. *Cancer Discov* *7*, 20-37.

597 Brown, J.T., Bai, X., and Johnson, A.W. (2000). The yeast antiviral proteins Ski2p,

598 Ski3p, and Ski8p exist as a complex in vivo. *Rna-a Publication of the Rna Society* *6*,

599 449.

600 Buisson, R., Langenbucher, A., Bowen, D., Kwan, E.E., Benes, C.H., Zou, L., and

601 Lawrence, M.S. (2019). Passenger hotspot mutations in cancer driven by APOBEC3A

602 and mesoscale genomic features. *Science* *364*.

603 Burgess, D.J. (2019). Switching APOBEC mutation signatures. *Nat Rev Genet* *20*,

604 253.

605 Burns, M.B., Lackey, L., Carpenter, M.A., Rathore, A., Land, A.M., Leonard, B.,

606 Refsland, E.W., Kotandeniya, D., Tretyakova, N., Nikas, J.B., *et al.* (2013a).

607 APOBEC3B is an enzymatic source of mutation in breast cancer. *Nature* *494*,

608 366-370.

- 609 Burns, M.B., Temiz, N.A., and Harris, R.S. (2013b). Evidence for APOBEC3B  
610 mutagenesis in multiple human cancers. *Nat Genet* 45, 977-983.
- 611 Cleary, J.M., Aguirre, A.J., Shapiro, G.I., and D'Andrea, A.D. (2020).  
612 Biomarker-Guided Development of DNA Repair Inhibitors. *Mol Cell* 78, 1070-1085.
- 613 Cvetkovic, M.A., Wurm, J.P., Audin, M.J., Schutz, S., and Sprangers, R. (2017). The  
614 Rrp4-exosome complex recruits and channels substrate RNA by a unique mechanism.  
615 *Nat Chem Biol* 13, 522-528.
- 616 Dai, L., Zhao, T., Bisteau, X., Sun, W., Prabhu, N., Lim, Y.T., Sobota, R.M., Kaldis, P.,  
617 and Nordlund, P. (2018). Modulation of Protein-Interaction States through the Cell  
618 Cycle. *Cell* 173, 1481-1494 e1413.
- 619 Dizon, D.S. (2017). PARP inhibitors for targeted treatment in ovarian cancer. *Lancet*  
620 390, 1929-1930.
- 621 Farmer, H., McCabe, N., Lord, C.J., Tutt, A.N., Johnson, D.A., Richardson, T.B.,  
622 Santarosa, M., Dillon, K.J., Hickson, I., Knights, C., *et al.* (2005). Targeting the DNA  
623 repair defect in BRCA mutant cells as a therapeutic strategy. *Nature* 434, 917-921.
- 624 Greaves, M. (2018). A causal mechanism for childhood acute lymphoblastic  
625 leukaemia. *Nat Rev Cancer* 18, 471-484.
- 626 Hutchinson, L. (2013). Genetics: Signatures of mutational processes in cancer-a big  
627 step closer. *Nat Rev Clin Oncol* 10, 545.
- 628 Januszyk, K., and Lima, C.D. (2014). The eukaryotic RNA exosome. *Curr Opin Struct*  
629 *Biol* 24, 132-140.
- 630 Jeggo, P.A., Pearl, L.H., and Carr, A.M. (2015). DNA repair, genome stability and  
631 cancer: a historical perspective. *Nature Reviews Cancer* 16, 35.
- 632 Jeggo, P.A., Pearl, L.H., and Carr, A.M. (2016). DNA repair, genome stability and  
633 cancer: a historical perspective. *Nat Rev Cancer* 16, 35-42.
- 634 Jonathan, H., John, L.C., and David, T. (2006). RNA-quality control by the exosome.  
635 *Nat Rev Mol Cell Biol* 7, 529-539.
- 636 Kandoth, C., McLellan, M.D., Vandin, F., Ye, K., Niu, B., Lu, C., Xie, M., Zhang, Q.,  
637 McMichael, J.F., Wyczalkowski, M.A., *et al.* (2013). Mutational landscape and  
638 significance across 12 major cancer types. *Nature* 502, 333-339.
- 639 Kilchert, C., Wittmann, S., and Vasiljeva, L. (2016). The regulation and functions of  
640 the nuclear RNA exosome complex. *Nat Rev Mol Cell Biol* 17, 227-239.
- 641 Li, S., Zhang, Y., Wang, N., Guo, R., Liu, Q., Lv, C., Wang, J., Wang, L., and Yang,

642 Q.K. (2020). Pan-cancer analysis reveals synergistic effects of CDK4/6i and PARPi  
643 combination treatment in RB-proficient and RB-deficient breast cancer cells. *Cell*  
644 *Death Dis* *11*, 219.

645 Lim, J., Giri, P.K., Kazadi, D., Laffleur, B., Zhang, W., Grinstein, V., Pefanis, E.,  
646 Brown, L.M., Ladewig, E., Martin, O., *et al.* (2017). Nuclear Proximity of Mtr4 to  
647 RNA Exosome Restricts DNA Mutational Asymmetry. *Cell* *169*, 523-537 e515.

648 Loeb, L.A. (2011). Human cancers express mutator phenotypes: origin, consequences  
649 and targeting. *Nat Rev Cancer* *11*, 450-457.

650 Lord, C.J., and Ashworth, A. (2012). The DNA damage response and cancer therapy.  
651 *Nature* *481*, 287-294.

652 Lord, C.J., and Ashworth, A. (2017). PARP inhibitors: Synthetic lethality in the clinic.  
653 *Science* *355*, 1152-1158.

654 Lorentzen, E., Basquin, J., Tomecki, R., Dziembowski, A., and Conti, E. (2008).  
655 Structure of the active subunit of the yeast exosome core, Rrp44: diverse modes of  
656 substrate recruitment in the RNase II nuclease family. *Molecular Cell* *29*, 717-728.

657 Malet, H., Topf, M., Clare, D.K., Ebert, J., Bonneau, F., Basquin, J., Drazkowska, K.,  
658 Tomecki, R., Dziembowski, A., Conti, E., *et al.* (2010). RNA channelling by the  
659 eukaryotic exosome. *EMBO Rep* *11*, 936-942.

660 McGranahan, N., Rosenthal, R., Hiley, C.T., Rowan, A.J., Watkins, T.B.K., Wilson,  
661 G.A., Birkbak, N.J., Veeriah, S., Van Loo, P., Herrero, J., *et al.* (2017). Allele-Specific  
662 HLA Loss and Immune Escape in Lung Cancer Evolution. *Cell* *171*, 1259-1271  
663 e1211.

664 Pearl, L.H., Schierz, A.C., Ward, S.E., Al-Lazikani, B., and Pearl, F.M. (2015).  
665 Therapeutic opportunities within the DNA damage response. *Nat Rev Cancer* *15*,  
666 166-180.

667 Pefanis, E., and Basu, U. (2015). RNA Exosome Regulates AID DNA Mutator  
668 Activity in the B Cell Genome. *Adv Immunol* *127*, 257-308.

669 Pefanis, E., Wang, J., Rothschild, G, Lim, J., Kazadi, D., Sun, J., Federation, A., Chao,  
670 J., Elliott, O., Liu, Z.P., *et al.* (2015). RNA exosome-regulated long non-coding RNA  
671 transcription controls super-enhancer activity. *Cell* *161*, 774-789.

672 Peng, L., Bian, X.W., Li, D.K., Xu, C., Wang, G.M., Xia, Q.Y., and Xiong, Q. (2015).  
673 Large-scale RNA-Seq Transcriptome Analysis of 4043 Cancers and 548 Normal  
674 Tissue Controls across 12 TCGA Cancer Types. *5*, 13413.

675 Petersen-Mahrt, S.K., Harris, R.S., and Neuberger, M.S. (2002). AID mutates *E. coli*  
676 suggesting a DNA deamination mechanism for antibody diversification. *Nature* *418*,  
677 99.

678 Petljak, M., Alexandrov, L.B., Brammell, J.S., Price, S., Wedge, D.C., Grossmann, S.,  
679 Dawson, K.J., Ju, Y.S., Iorio, F., Tubio, J.M.C., *et al.* (2019). Characterizing  
680 Mutational Signatures in Human Cancer Cell Lines Reveals Episodic APOBEC  
681 Mutagenesis. *Cell* *176*, 1282-1294 e1220.

682 Quansheng, L., Greimann, J.C., and Lima, C.D. (2006). Reconstitution, activities, and  
683 structure of the eukaryotic RNA exosome. *Cell* *127*, 1223-1237.

684 Roberts, S.A., and Gordenin, D.A. (2014). Hypermutation in human cancer genomes:  
685 footprints and mechanisms. *Nat Rev Cancer* *14*, 786-800.

686 Robertson, A.G., Kim, J., Al-Ahmadie, H., Bellmunt, J., Guo, G., Cherniack, A.D.,  
687 Hinoue, T., Laird, P.W., Hoadley, K.A., Akbani, R., *et al.* (2017). Comprehensive  
688 Molecular Characterization of Muscle-Invasive Bladder Cancer. *Cell* *171*, 540-556  
689 e525.

690 Roos, W.P., Thomas, A.D., and Kaina, B. (2015). DNA damage and the balance  
691 between survival and death in cancer biology. *Nature Reviews Cancer* *16*, 20.

692 Roos, W.P., Thomas, A.D., and Kaina, B. (2016). DNA damage and the balance  
693 between survival and death in cancer biology. *Nat Rev Cancer* *16*, 20-33.

694 Sale, J.E., Calandrini, D.M., Takata, M., , Takeda, S., , and Neuberger, M.S. (2001).  
695 Ablation of XRCC2/3 transforms immunoglobulin V gene conversion into somatic  
696 hypermutation. *Nature* *412*, 921-926.

697 Schaaper, R.M., and Dunn, R.L. (1987). Spectra of spontaneous mutations in  
698 *Escherichia coli* strains defective in mismatch correction: the nature of in vivo DNA  
699 replication errors. *Proceedings of the National Academy of Sciences of the United*  
700 *States of America* *84*, 6220-6224.

701 Song, C., Wang, L., Wu, X., Wang, K., Xie, D., Xiao, Q., Li, S., Jiang, K., Liao, L.,  
702 Yates, J.R., 3rd, *et al.* (2018). PML Recruits TET2 to Regulate DNA Modification and  
703 Cell Proliferation in Response to Chemotherapeutic Agent. *Cancer Res* *78*,  
704 2475-2489.

705 Thoma, C.R., Toso, A., Gutbrodt, K.L., Reggi, S.P., Frew, I.J., Schraml, P., Hergovich,  
706 A., Moch, H., Meraldi, P., and Krek, W. (2009). VHL loss causes spindle  
707 misorientation and chromosome instability. *Nat Cell Biol* *11*, 994-1001.

- 708 Tomecki, R., Drazkowska, K., and Dziembowski, A. (2010). Mechanisms of RNA  
709 degradation by the eukaryotic exosome. *Chembiochem* *11*, 938-945.
- 710 Tubbs, A., and Nussenzweig, A. (2017). Endogenous DNA Damage as a Source of  
711 Genomic Instability in Cancer. *Cell* *168*, 644-656.
- 712 Tutt, A., Robson, M., Garber, J.E., Domchek, S.M., Audeh, M.W., Weitzel, J.N.,  
713 Friedlander, M., Arun, B., Loman, N., Schmutzler, R.K., *et al.* (2010). Oral  
714 poly(ADP-ribose) polymerase inhibitor olaparib in patients with BRCA1 or BRCA2  
715 mutations and advanced breast cancer: a proof-of-concept trial. *Lancet* *376*, 235-244.
- 716 Uhlen, M., Zhang, C., Lee, S., Sjostedt, E., Fagerberg, L., Bidkhori, G., Benfeitas, R.,  
717 Arif, M., Liu, Z., Edfors, F., *et al.* (2017). A pathology atlas of the human cancer  
718 transcriptome. *Science* *357*.
- 719 Ulmke, P.A., Xie, Y., Sokpor, G., Pham, L., Shomroni, O., Berulava, T., Rosenbusch,  
720 J., Basu, U., Fischer, A., Nguyen, H.P., *et al.* (2021). Post-transcriptional regulation by  
721 the exosome complex is required for cell survival and forebrain development via  
722 repression of P53 signaling. *Development* *148*.
- 723 Wang, L., Song, C., Wang, N., Li, S., Liu, Q., Sun, Z., Wang, K., Yu, S.C., and Yang,  
724 Q. (2020). NADP modulates RNA m(6)A methylation and adipogenesis via enhancing  
725 FTO activity. *Nat Chem Biol* *16*, 1394-1402.
- 726 Wasmuth, E.V., Kurt, J., and Lima, C.D. (2014). Structure of an Rrp6-RNA exosome  
727 complex bound to poly(A) RNA. *Nature* *511*, 435-439.
- 728 Weinstein, J.N., Collisson, E.A., Mills, G.B., Shaw, K.R., Ozenberger, B.A., Ellrott,  
729 K., Shmulevich, I., Sander, C., and Stuart, J.M. (2013). The Cancer Genome Atlas  
730 Pan-Cancer analysis project. *Nature genetics* *45*, 1113-1120.
- 731 Yang, Q., Deng, X., Lu, B., Cameron, M., Fearn, C., Patricelli, M.P., Yates, J.R., 3rd,  
732 Gray, N.S., and Lee, J.D. (2010). Pharmacological inhibition of BMK1 suppresses  
733 tumor growth through promyelocytic leukemia protein. *Cancer Cell* *18*, 258-267.
- 734 Zhang, J., Wu, T., Simon, J., Takada, M., Saito, R., Fan, C., Liu, X.D., Jonasch, E.,  
735 Xie, L., Chen, X., *et al.* (2018). VHL substrate transcription factor ZHX2 as an  
736 oncogenic driver in clear cell renal cell carcinoma. *Science* *361*, 290-295.
- 737 Zhang, Y., Ng, K.S., Kucherlapati, M., Chen, F., Liu, Y., Tsang, Y.H., Velasco, G.D.,  
738 Kang, J.J., Akbani, R., and Hadjipanayis, A. (2017). A Pan-Cancer Proteogenomic  
739 Atlas of PI3K/AKT/mTOR Pathway Alterations. *Cancer Cell* *31*, 820.
- 740 Zhou, S.L., Zhou, Z.J., Hu, Z.Q., Song, C.L., Luo, Y.J., Luo, C.B., Xin, H.Y., Yang,

741 X.R., Shi, Y.H., Wang, Z., *et al.* (2019). Genomic sequencing identifies WNK2 as a  
742 driver in hepatocellular carcinoma and a risk factor for early recurrence. *J Hepatol* 71,  
743 1152-1163.

## Figure legends

**Figure 1.** Identification of candidate ESMs in KIRC by statistical analyses. **(A)** Schematic of this study. **(B)** Illustration of base substitutions. **(C)** Schematic showing the archaeal and eukaryotic exosome complexes viewed from the top. **(D)** Summary statistics for the 6 types of c-substitutions in KIRC. **(E)** Scatter plots showing the correlation between the rank of mutation and gene expression. Each plot represents one KIRC sample. The orange dashed line shows the best fit for visualization. *P* values were calculated by spearman's rank correlation. **(F)** Volcano plots of *p* and *r* values calculated by spearman correlation analyses. Each plot represents one gene. The top 1% of genes were taken as candidates and marked in red. **(G)** Box plots showing ASNS expression in the high and low C>A/G>T mutation groups. The expression was normalized to TBP. **(H)** Volcano plots showing the *p* and fold change (FC) values calculated by the two-tailed student's *t*-test. Each plot represents one gene. FC was calculated by the formula: FC = the mean gene expression in the high group/that in the low group. The top 1% genes were taken as candidates and marked in red. **(I)** C-substitution mutation frequencies in 5 types of major cancers. **(J, K)** Mutation spectra of the TP53 gene in BRCA **(J)** and VHL gene in KIRC **(K)**. **(L)** Kaplan-Meier (KM) analyses of OS between VHL C>A/G>T and C>T/G>A mutation groups. The median OSs in the C>A/G>T and C>T/G>A groups were 72.95 and 108.91 months, respectively. The *p* value was obtained from the log-rank test. **(M)** Venn diagram showing the overlap of the candidate genes identified by three types of statistical analyses as noted.



# Figure 1

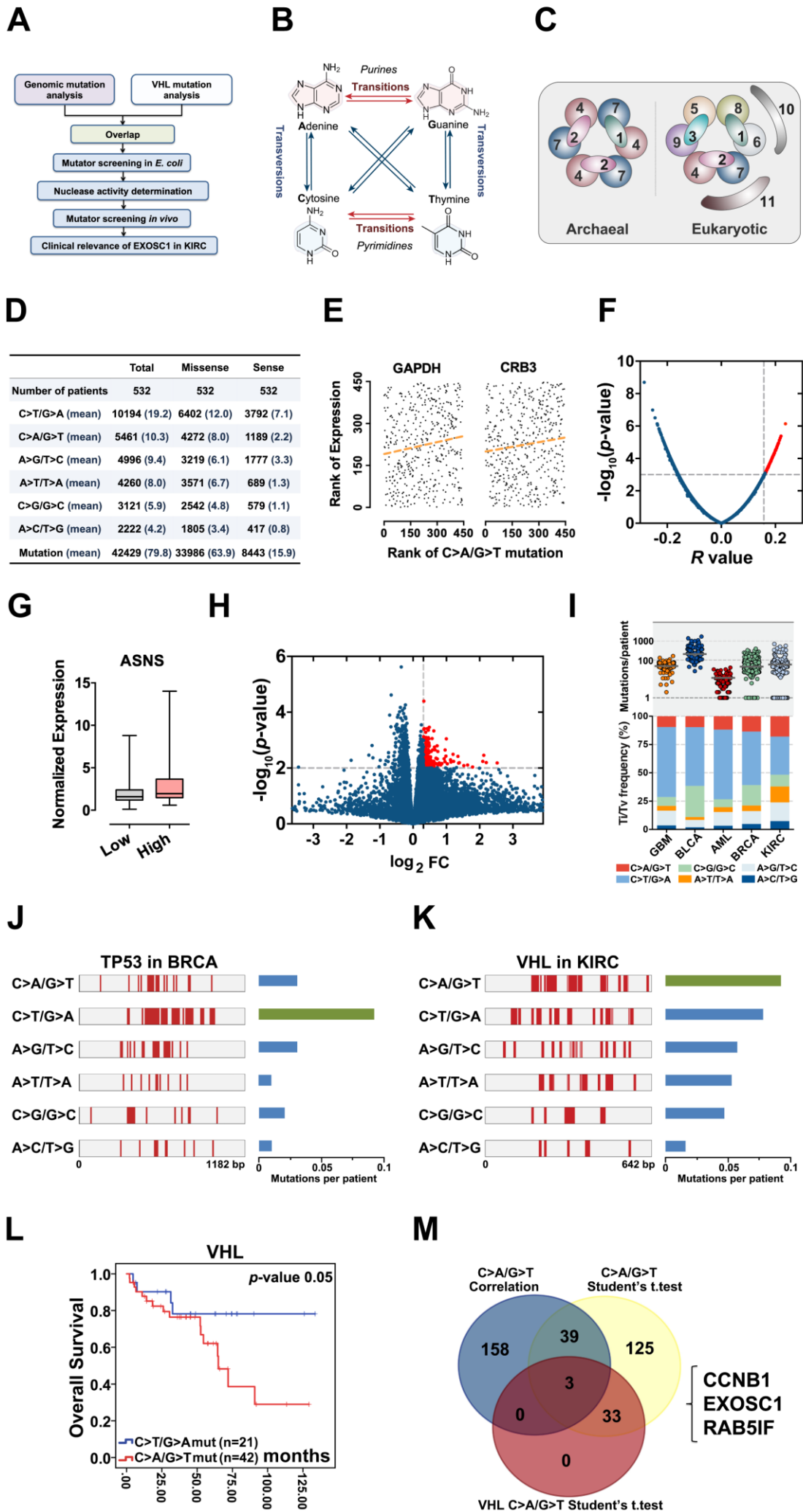


**Figure 2.** EXOSC1 promotes mutations in *E. coli*. **(A)** Western blot showing His-tagged protein levels in *E. coli*. **(B, C)** The frequencies of the Rif<sup>R</sup> mutation in the *E. coli* cells expressing candidate ESMs **(B)** or exosome family members **(C)**. The vector and AID were used as negative and positive controls, respectively. Each plot represents the mutational frequency of an independent overnight culture (n=30). Median mutational frequency of the gene is noted. **(D)** Frequencies of the Rif<sup>R</sup> mutation in the *E. coli* cells treated with and without IPTG (n=30). **(E, F)** Representative images of *E. coli* cells treated with **(E)** and without **(F)** IPTG. **(G)** The mutational distribution in 25 independent Rif<sup>R</sup> colonies transformed by vector or EXOSC1. **(H, I)** Summary of the c-substitutions in Rif<sup>R</sup> colonies transformed by vector **(H)** and EXOSC1 **(I)**. **(J)** The mutational frequencies of each c-substitution in Rif<sup>R</sup> colonies. The *p* value was calculated by fisher's exact-test.

# Figure 2

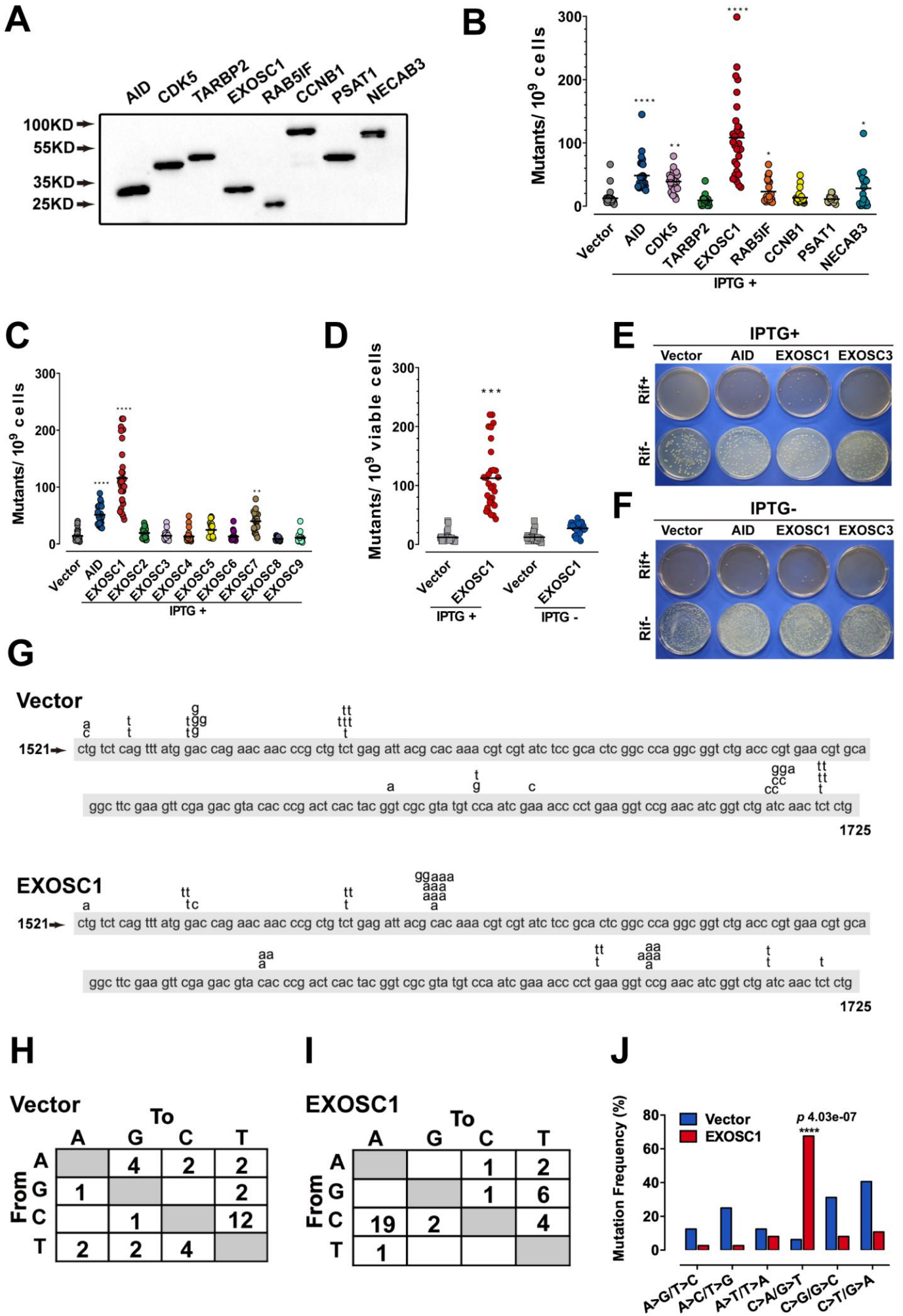


**Figure 3.** EXOSC1 cleaves ssDNA. **(A)** Coomassie blue staining of *in vitro* purified EXOSC1 protein. **(B)** Schematic of synthetic DNA substrates. **(C)** *In vitro* cleavage assays of EXOSC1 using generic ssDNA, dsDNA and DNA-RNA hybrid as substrates. The assays were performed in the presence of 1  $\mu$ M oligonucleotides, 1  $\mu$ M EXOSC1, 70 mM KCl, 700  $\mu$ M MgCl<sub>2</sub>, 1 mM DTT, and 20 mM Tris-HCl pH 7.0. After incubation at 37 °C for 4 h, resultant samples were analyzed by 15% polyacrylamide TBE-urea gels. **(D)** Cleavage assays of EXOSC1 in the presence or absence of EXOSC3, EXOSC6, EXOSC7 and EXOSC8 using generic ssDNA as substrates. **(E)** Cleavage assays in the presence of the components as noted. **(F)** Cleavage assays of EXOSC1 at the pH as noted. **(G)** Time course cleavage assays of EXOSC1 using generic ssDNA as substrates. **(H)** Rate curve of EXOSC1 cleavage at 37 °C and pH 7.0.

# Figure 3

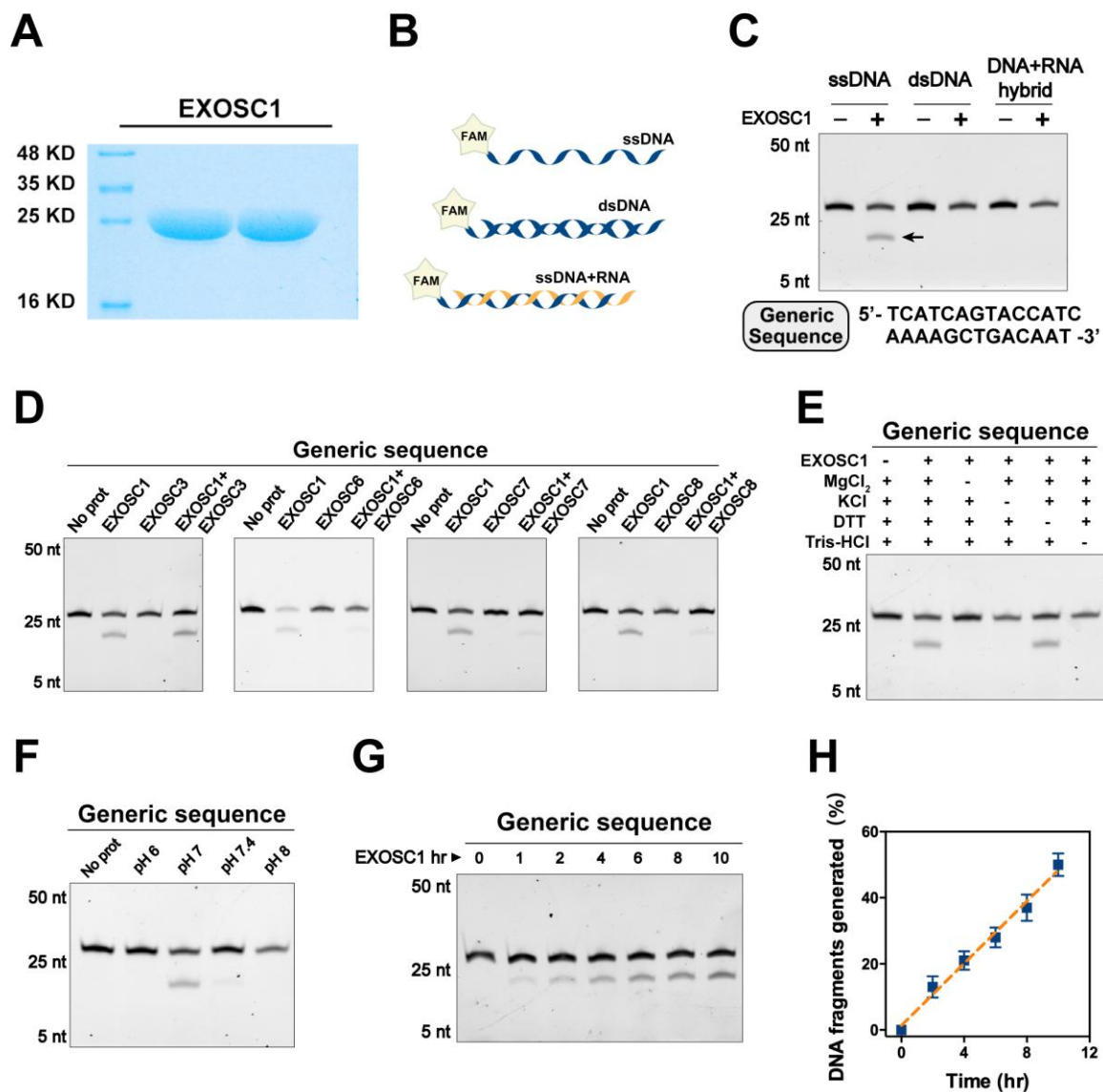


**Figure 4.** EXOSC1 prefers to cleave C sites in ssDNA. **(A, B)** Cleavage assay of EXOSC1 using unbiased DNA, dsDNA and DNA-RNA hybrid as substrates. **(C, D)** Cleavage assays of EXOSC1, EXOSC3, EXOSC7 and EXOSC8 using unbiased ssDNA as substrates. **(E)** Mass spectrometry (MS) analyses of the resultant mixtures described in **(B)**. C, G, A and T were detected by MS using nucleoside to base ion mass transitions of 228.1 to 112.2 (C), 268.1 to 152.1 (G), 252.2 to 136.1 (A), and 243.1 to 127.2 (T) (Supplementary Figure 3E). Standard curves were generated by a serial dilution of C, G, A and T (Supplementary Figure 3F). Free C, G, A and T contained in the reaction mixtures were quantified by standard curves. **(F)** Schematic showing that the consequence of C>A mutation in the coding strand is distinct from that in the template strand. **(G)** Correlation between EXOSC1 expression and the c-substitution mutation as noted in KIRC. Each line represents one best fit for visualization. *P* values were from spearman's rank correlation. *P* and *r* values of C>A mutations were 0.0001 and 0.19, respectively; C>A/G>T: *p* = 0.0006, *r* = 0.17; G>T: *p* = 0.0271, *r* = 0.10; total mutations: *p* = 0.0594, *r* = 0.09; C/G>G/C: *p* = 0.5730, *r* = 0.03. **(H)** Student's *t*-tests analyses of the expression difference of EXOSC1 between the high and low mutation groups. FC = the mean gene expression in the high group/that in the low group.

# Figure 4

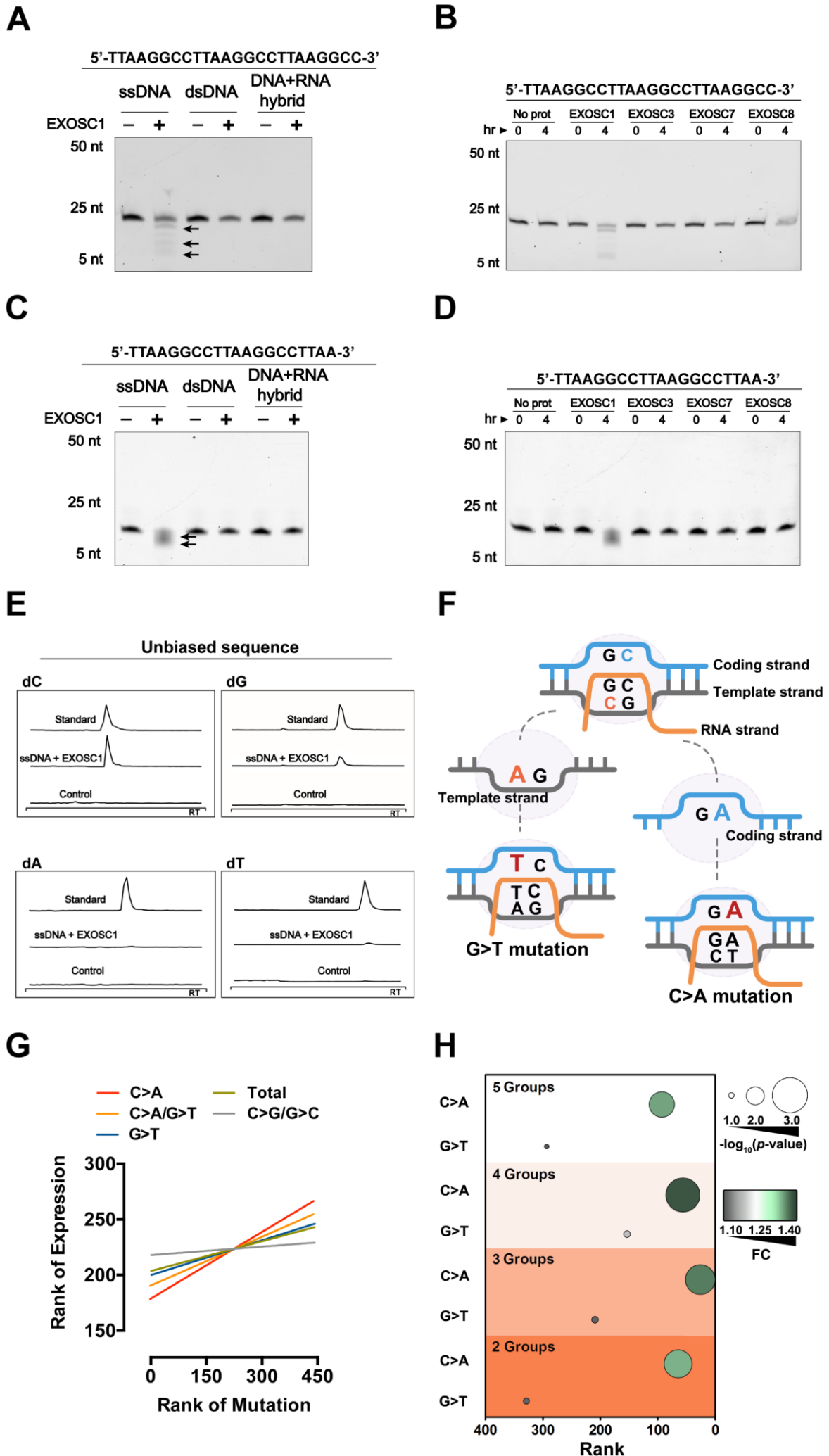


**Figure 5.** EXOSC1 enhances DNA damages and mutations in KIRC Cells. **(A)** Representative fluorescent images of  $\gamma$ -H2AX foci in 769-P cells transfected with control (pCDH, empty vector) or pCDH-Flag EXOSC1 plasmids for 2 days. Scale bar = 10  $\mu$ m. **(B)** Percentage of cells with more than 20  $\gamma$ -H2AX foci in the KIRC cells transfected with control or pCDH-Flag EXOSC1 plasmids for 2 days. **(C)** Percentage of cells with more than 20  $\gamma$ -H2AX foci in the KIRC cells infected with lentivirus encoding shRNAi control (pLKO scramble) or pLKO sh-EXOSC1 for 2 days. **(D)** Representative images of DNA comets in 769-P cells transfected with control or pCDH-Flag EXOSC1 plasmids for 2 days. **(E)** Comet tail moment of the 769-P and TUHR14TKB cells transfected with control or pCDH-Flag EXOSC1 plasmids for 2 days. **(F)** 3D-PCR and subsequent sequencing analyses of the VHL mutations in the TUHR14TKB cells stably expressing control (vector) or EXOSC1 (pCDH-Flag EXOSC1, EXOSC1-OE). **(G)** 3D-PCR analyses of VHL in TUHR14TKB cells stably expressing control (pLKO.1 vector) or shRNA against EXOSC1 (pLKO shEXOSC1-1, EXOSC1-KD). **(H)** 3D-PCR analyses of VHL in TUHR14TKB cells stably expressing control, EXOSC1-OE and/or shRNA against XRCC1 (pMKO.1 shXRCC1-1, XRCC1-KD). **(I)** 3D-PCR analyses of VHL in TUHR14TKB cells stably expressing control (pLKO.1 vector), shRNA against EXOSC1 (pLKO shEXOSC1-1, EXOSC1-KD) and/or shRNA against XRCC1 (pMKO.1 shXRCC1-1, XRCC1-KD). **(J)** Schematic showing the subcutaneous xenograft tumor models. The  $5 \times 10^6$  control, EXOSC1-OE and EXOSC1-KD 769-P cells were implanted subcutaneously. After 2 weeks, the resultant tumors were analyzed by 3D-PCR. **(K)** 3D-PCR analyses of VHL in the tumors described in **(J)**.



# Figure 5

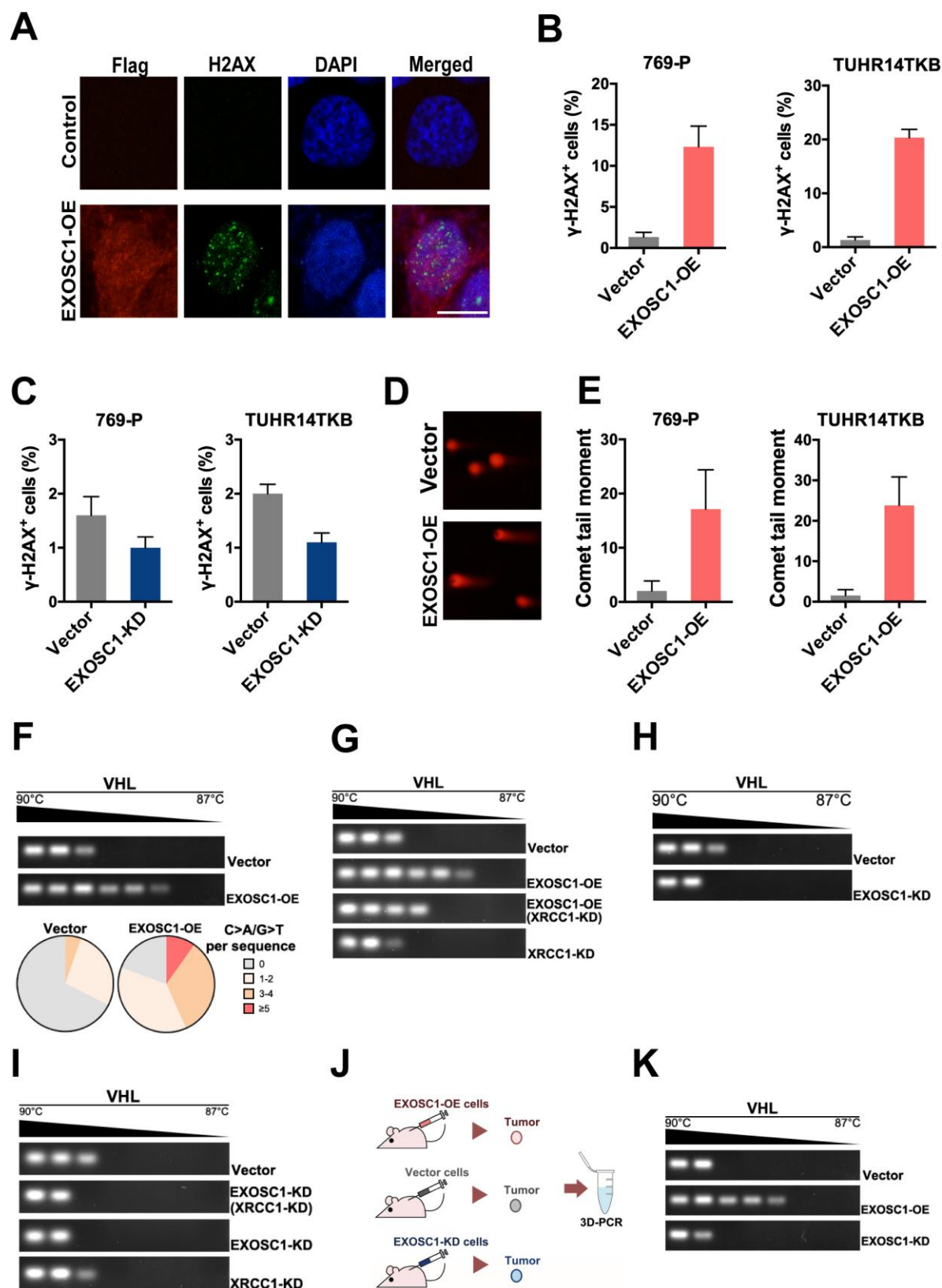
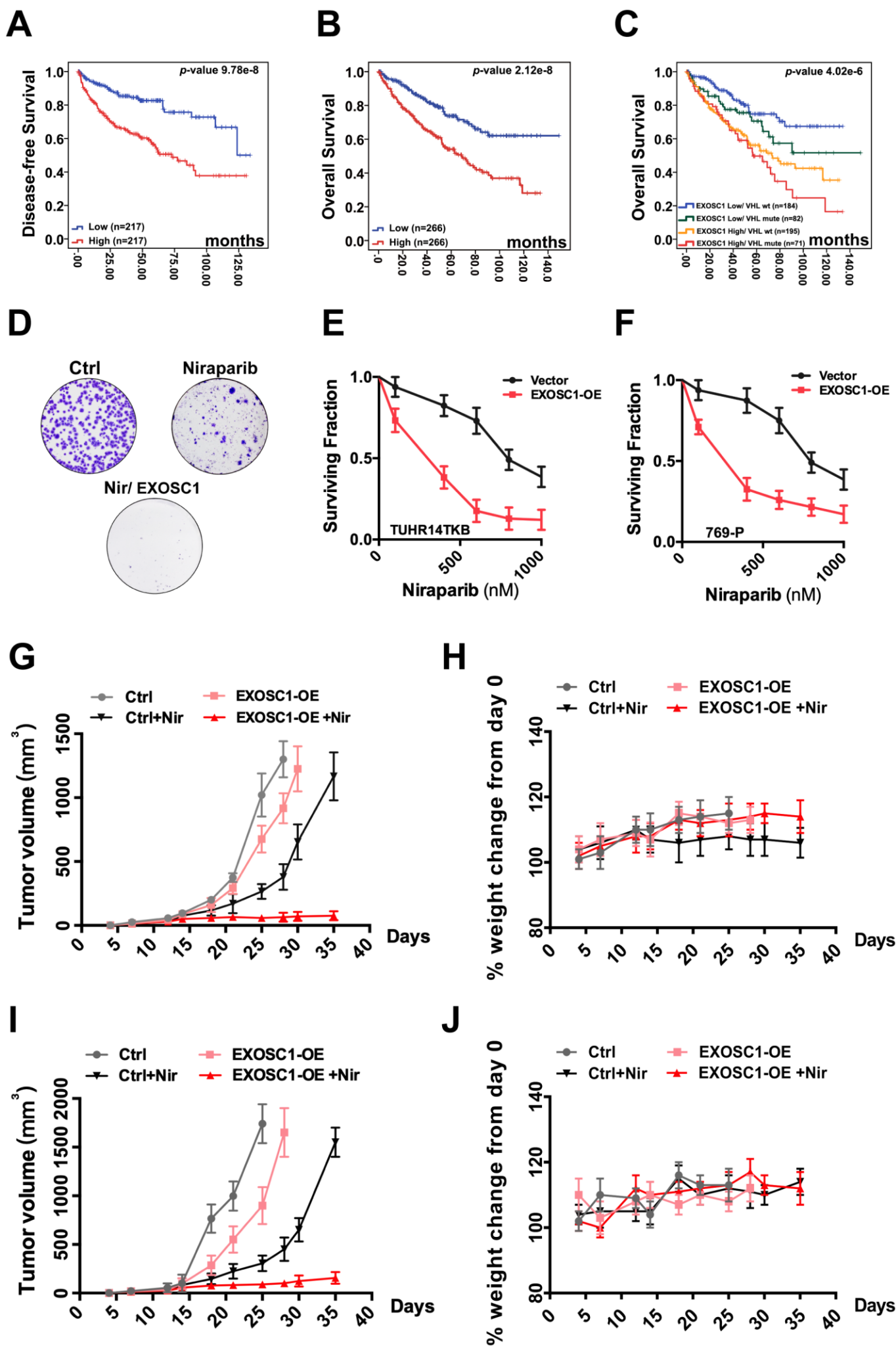


**Figure 6.** EXOSC1 sensitizes KIRC cells to PARP inhibitor. **(A, B)** KM analyses of DFS **(A)** and OS **(B)** in KIRC patients with different EXOSC1 levels. *P* values were obtained from the log-rank test. **(C)** KM analysis of OS in KIRC patients with different EXOSC1 expression levels and VHL mutations. **(D)** Colony formation of control and EXOSC1-OE TUHR14TKB cells treated with 600 nM niraparib. **(E, F)** Clonogenic survival of control and EXOSC1-OE TUHR14TKB **(E)** and 769-P **(F)** cells treated with niraparib. **(G, I)** Tumor volumes of 769-P **(G)** and Caki-2 **(I)** xenografts treated with or without niraparib. *n* = 4 groups; *n* = 6 mice/group; ± SEM. **(H, J)** Body weight change percentage of 769-P **(H)** and Caki-2 **(J)** xenografts treated as described in **(G)**.

# Figure 6



## Supplementary Figure Legends

**Figure 1—figure supplement 1.** Identification of candidate ESMs in KIRC by statistical analyses. (A and B) Mutation spectra of TP53 (A) and VHL (B) normalized by the nucleotide abundance.

# Figure 1—figure supplement 1

**A**

**B**

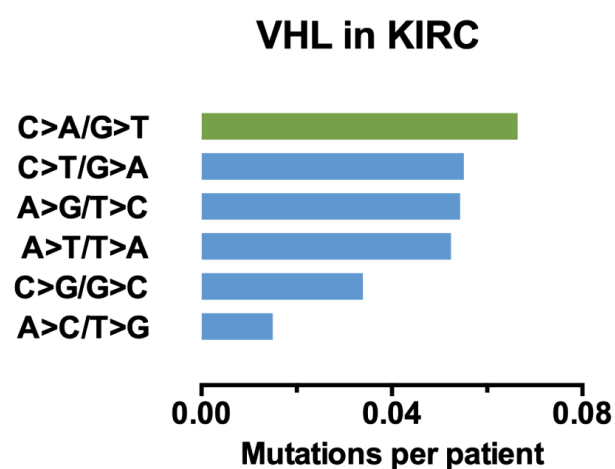
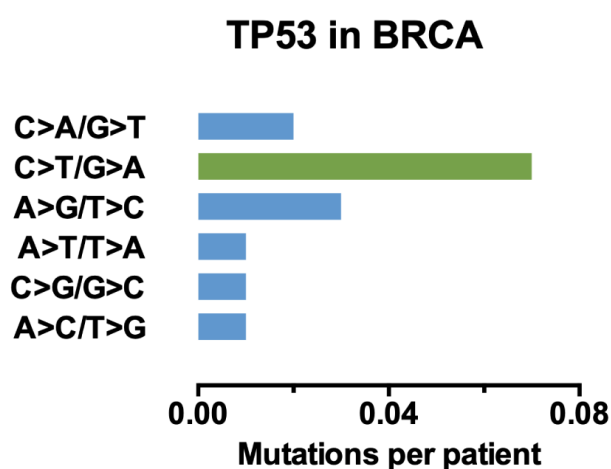


**Figure 2—figure supplement 1.** EXOSC1 promotes mutations in *E. coli*. (A) Setup plot showing the overlap numbers of the candidate genes of the 6 types of c-substitutions. More details can be found in Supplementary Table S4. (B) Western blot showing the His-tagged protein levels of the exosome complex members in the *E. coli* cells. (C) Growth rates of control and EXOSC1-transformed cells in the presence of IPTG. n = 5. (D) Frequencies of c-substitutions in Rif<sup>R</sup> colonies were normalized to the nucleotide abundances. The *p* value was calculated by fisher's exact test.

## Figure 2—figure supplement 1

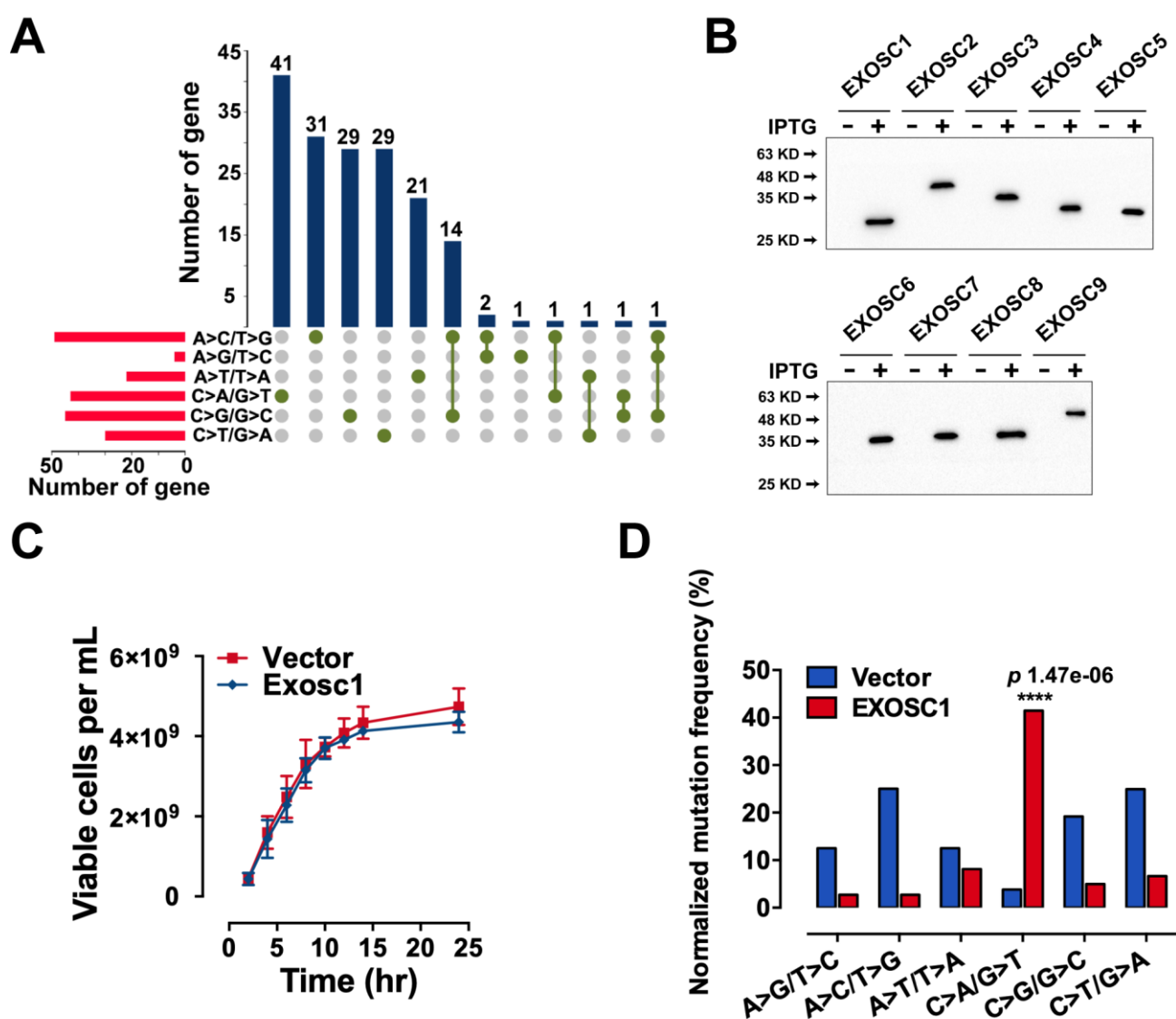
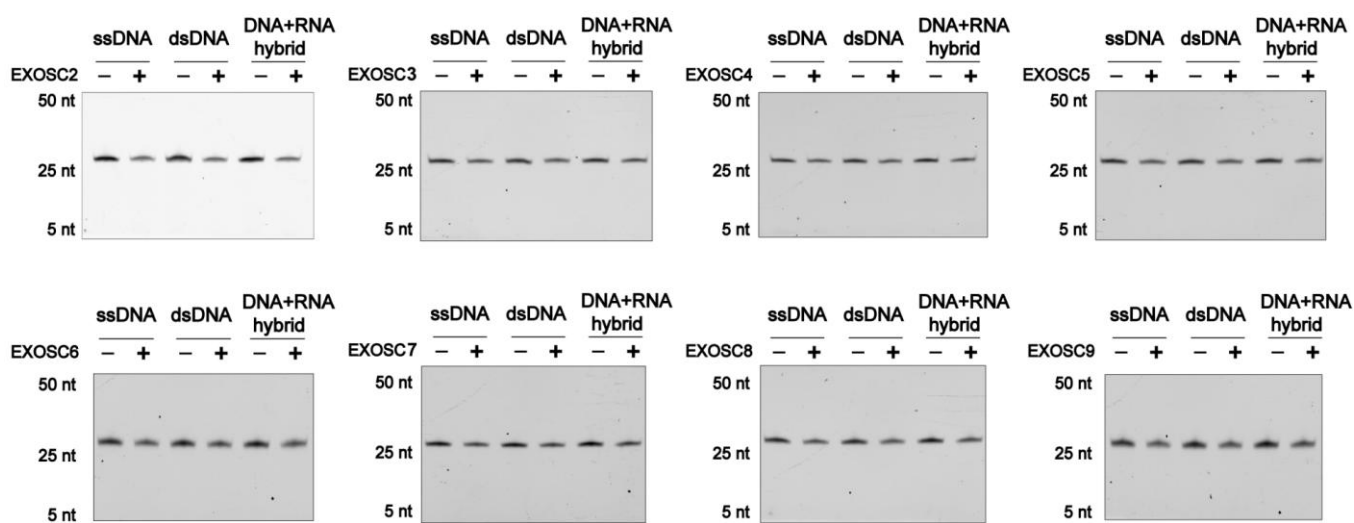


**Figure 3—figure supplement 1.** EXOSC1 cleaves ssDNA. (A) *In vitro* cleavage assays of EXOSC1 homologs (EXOSC2–EXOSC9) using generic ssDNA, dsDNA and DNA-RNA hybrid as substrates. (B) Cleavage assays of EXOSC1 in the presence/absence of EXOSC2, EXOSC4, EXOSC5 or EXOSC9.

# Figure 3—figure supplement 1

**A**



**B**

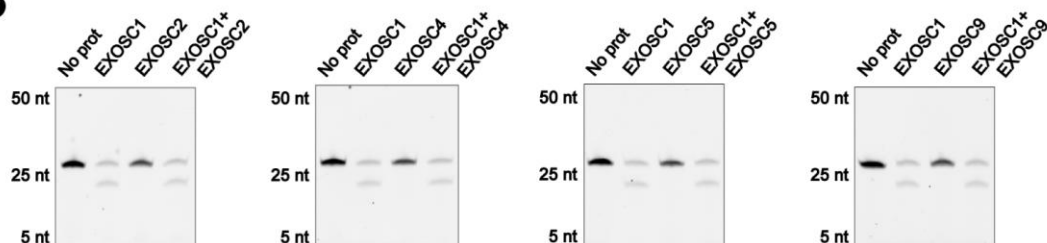
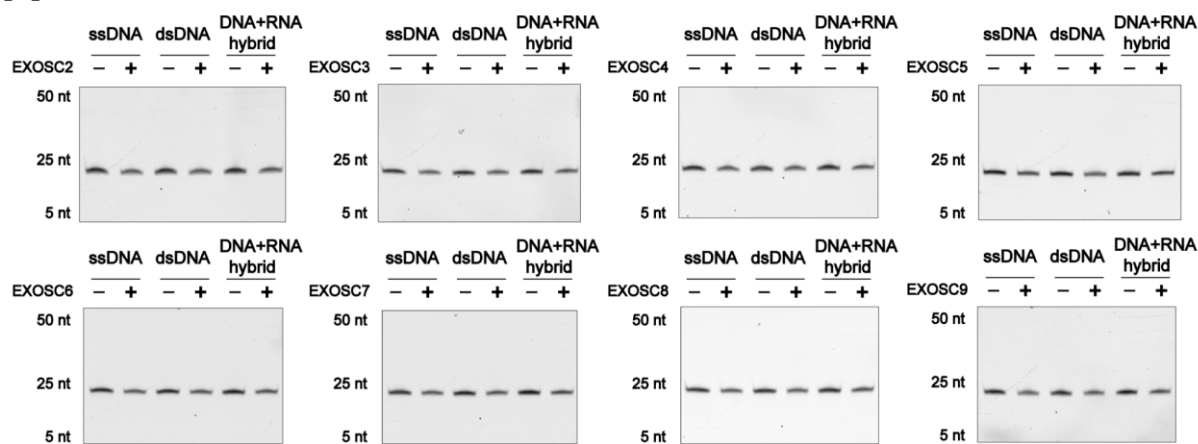


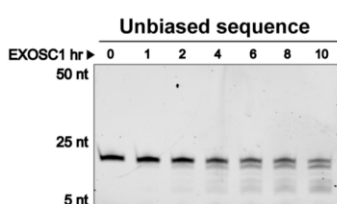
**Figure 4—figure supplement 1.** EXOSC1 prefers to cleave C sites in ssDNA. **(A)** Cleavage assays of EXOSC2-EXOSC9 using unbiased ssDNA, dsDNA and DNA-RNA hybrid as substrates. **(B)** Time course cleavage assays of EXOSC1 using unbiased ssDNA as substrates. **(C)** Base ion mass transitions for LC-MS/MS analyses of C, G, A and T. Free nucleosides were detected using nucleoside to base ion mass transitions of 228.1 to 112.2 (C), 268.1 to 152.1 (G), 252.2 to 136.1 (A), and 243.1 to 127.2 (T). **(D)** LC-MS/MS standard curves of nucleoside as noted. **(E and F)** Frequencies **(E)** and normalized frequencies **(F)** of 12 types of substitutions in Rif<sup>R</sup> colonies. *P* values were calculated using fisher's exact test. **(G)** Correlation between EXOSC1 expression and the mutation as noted in KIRC. Each plot represents one KIRC sample. **(H)** Student's *t*-test analyses of EXOSC1 expression difference between the high and low mutation groups. The 532 KIRC patients were grouped into 2, 3, 4 or 5 groups to evaluate the impact of group number. **(I and J)** Summary statistics for the mutation as noted in KIRC. *P* values were calculated by the two-tailed student's *t*-test.

# Figure 4—figure supplement 1

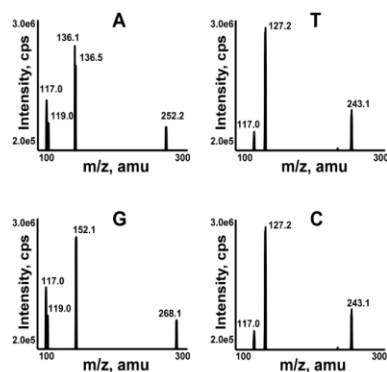
**A**



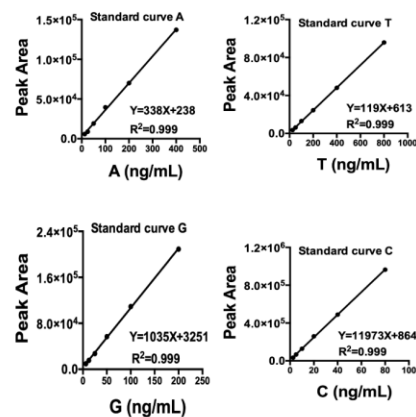
**B**



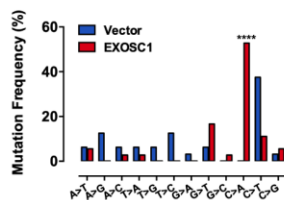
**C**



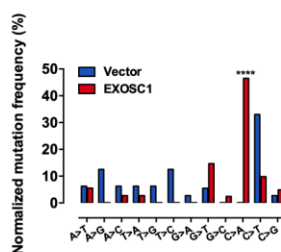
**D**



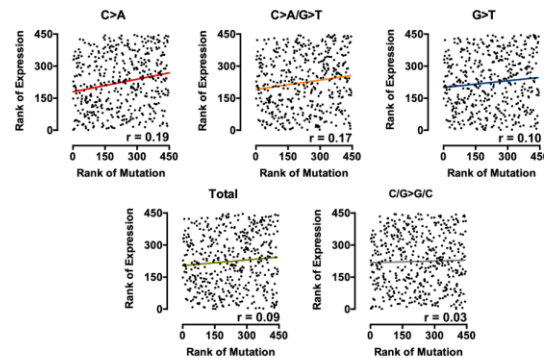
**E**



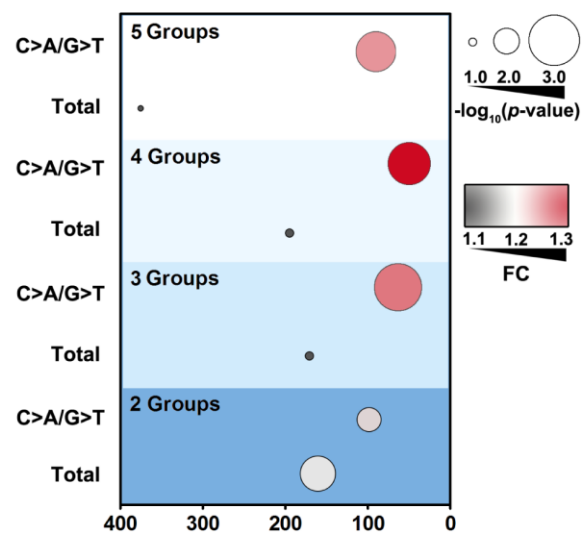
**F**



**G**



**H**



**I**

P value	C>A/G>T	Total
2-groups	0.0340	0.0078
3-groups	0.0004	0.0186
4-groups	0.0008	0.0419
5-groups	0.0054	0.1553

**J**

P value	C>A	G>T
2-groups	0.0001	0.0510
3-groups	0.0001	0.0210
4-groups	0.0001	0.0226
5-groups	0.0008	0.0437



**Figure 5—figure supplement 1.** EXOSC1 enhances DNA damages and mutations in KIRC cells. (A) Western blot analyses of EXOSC1 in stable control, enhanced EXOSC1, and EXOSC1 knockdown cells. (B) Quantitative PCR analyses of EXOSC1 mRNA in the 769-P cells stably expressing shRNA (pLKO EXOSC1-1 or pLKO EXOSC1-2) against EXOSC1. (C) Representative fluorescence images of  $\gamma$ -H2AX foci in the 769-P cells stably expressing shRNA against control (empty vector) or EXOSC1 (pLKO EXOSC1-1, EXOSC1-KD). Scale bar = 10  $\mu$ m. (D and F) Western blot analyses of EXOSC1 and XRCC1 protein levels in the stable cells as noted. (E) Quantitative PCR analyses of the mRNA in the cells stably expressing shRNA against EXOSC1 and/or XRCC1.

## Figure 5—figure supplement 1

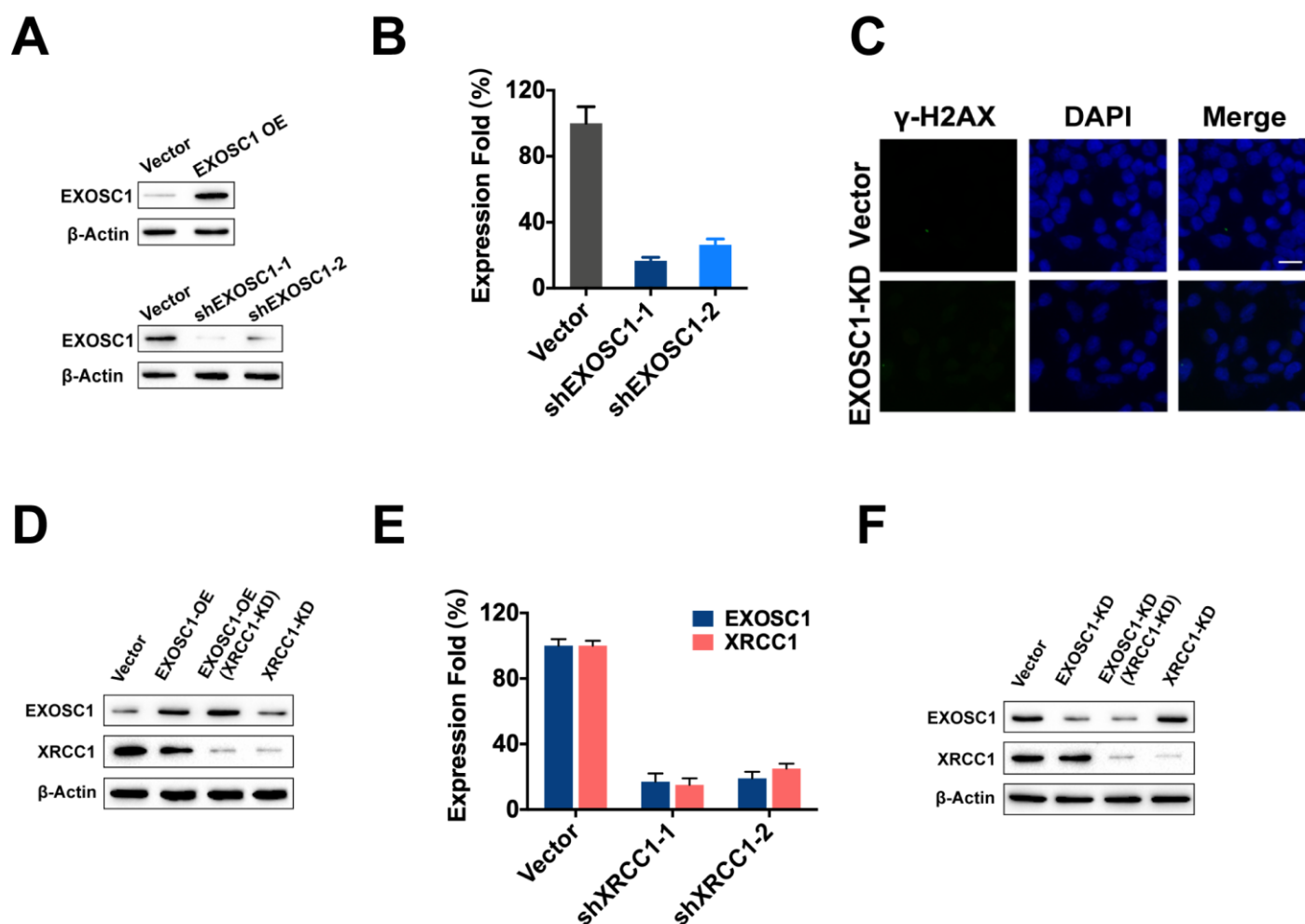


**Figure 6—figure supplement 1.** EXOSC1 sensitizes KIRC cells to PARP inhibitor. **(A)** The fragments per kilo base per million mapped reads (FPKM) of the noted gene in 532 KIRC. Each dot represents one KIRC patient. **(B)** Best separation KM analyses of OS in KIRC patients with different EXOSC1 levels. The median OS (the low vs high EXOSC1 group) = 106.40 vs 71.91 months. **(C)** Summary statistics for Figure 6C. **(D)** Clonogenic survival of control/EXOSC1-OE SNU-1272 and Caki-2 cells treated with niraparib.

# Figure 6—figure supplement 1

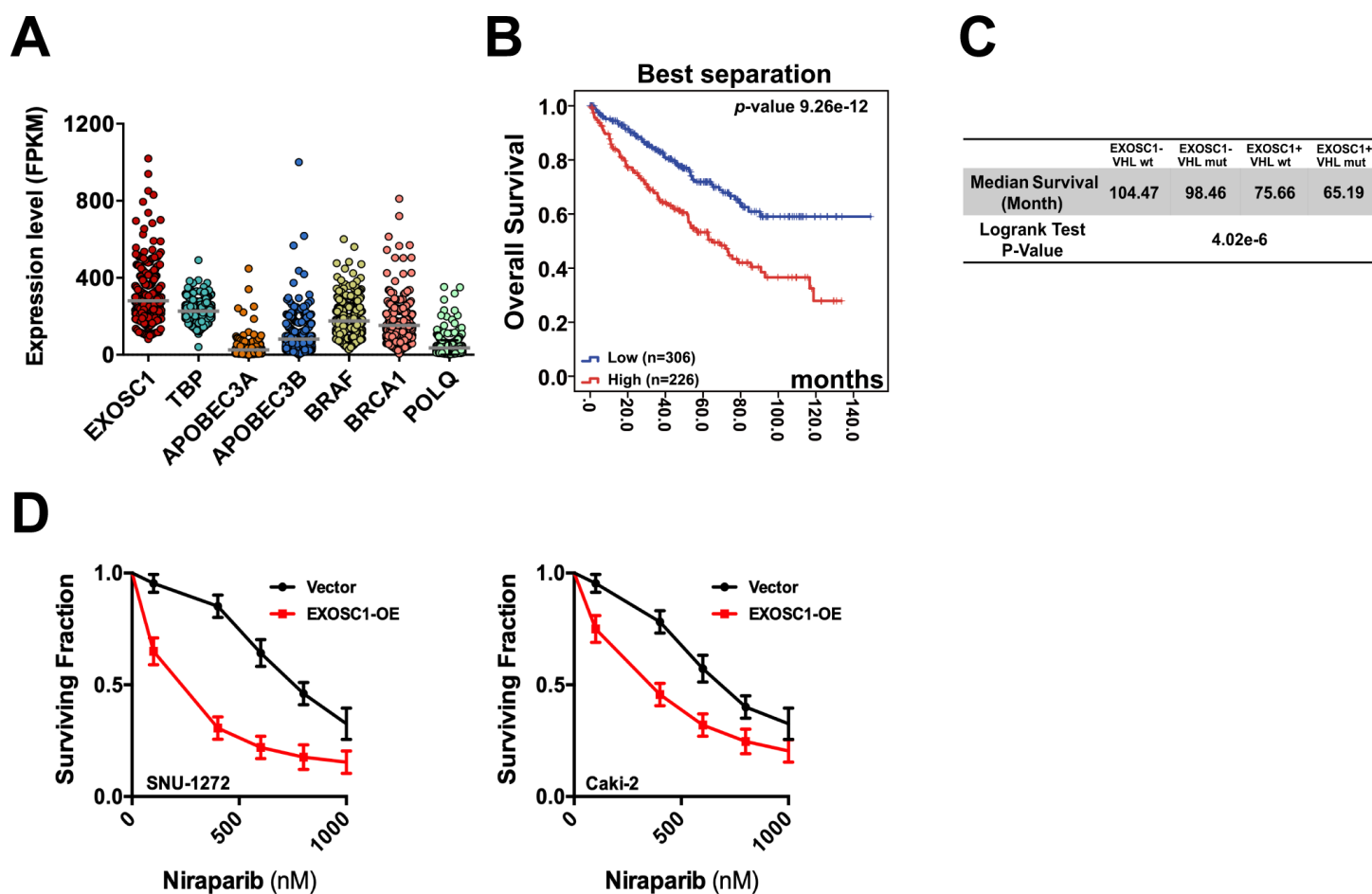
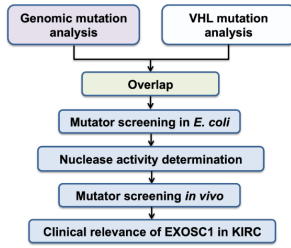
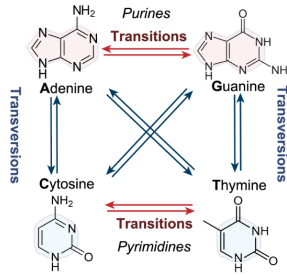


# Figure 1

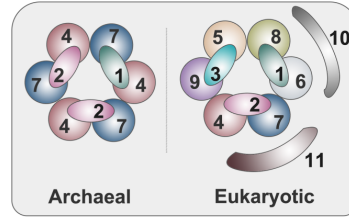
**A**



**B**



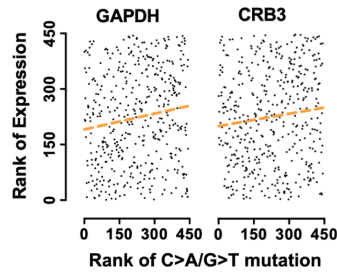
**C**



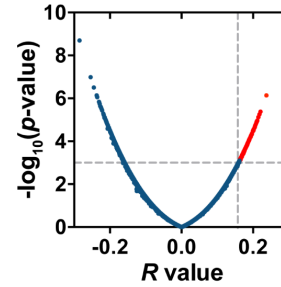
**D**

	Total	Missense	Sense
Number of patients	532	532	532
C>T/G>A (mean)	10194 (19.2)	6402 (12.0)	3792 (7.1)
C>A/G>T (mean)	5461 (10.3)	4272 (8.0)	1189 (2.2)
A>G/T>C (mean)	4996 (9.4)	3219 (6.1)	1777 (3.3)
A>T/T>A (mean)	4260 (8.0)	3571 (6.7)	689 (1.3)
C>G/G>C (mean)	3121 (5.9)	2542 (4.8)	579 (1.1)
A>C/T>G (mean)	2222 (4.2)	1805 (3.4)	417 (0.8)
Mutation (mean)	42429 (79.8)	33986 (63.9)	8443 (15.9)

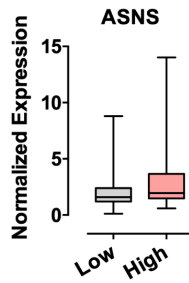
**E**



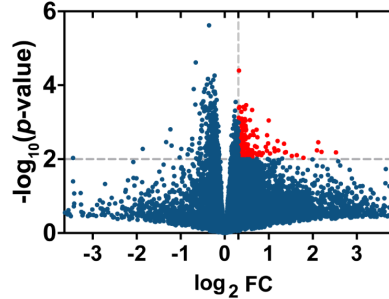
**F**



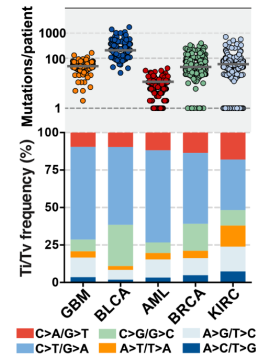
**G**



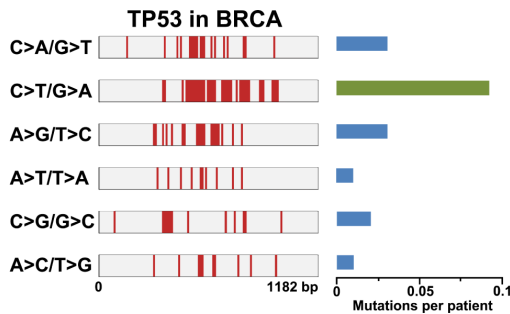
**H**



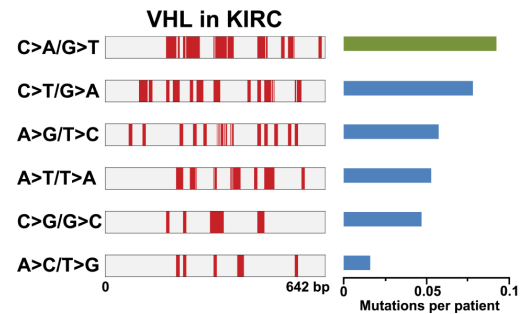
**I**



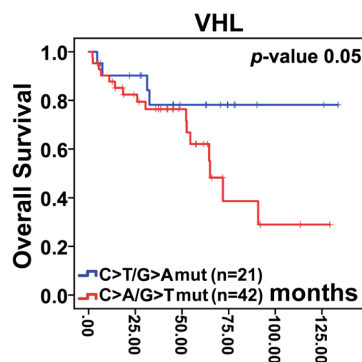
**J**



**K**



**L**



**M**

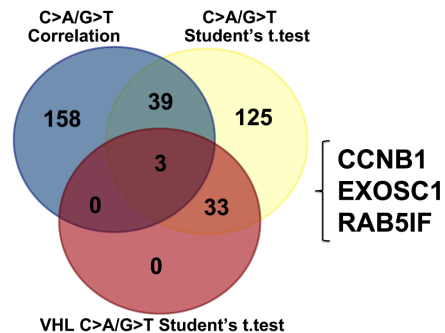
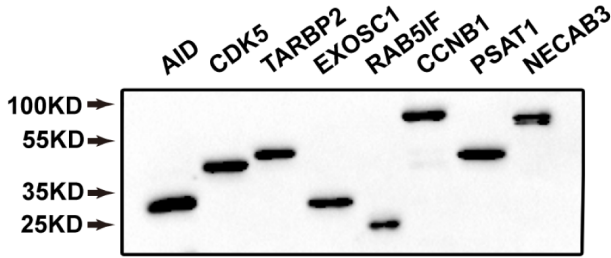
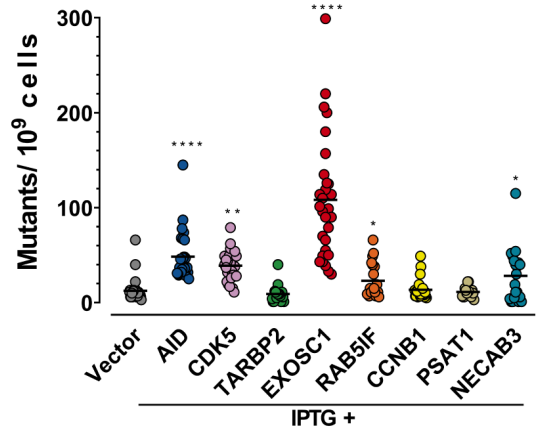


# Figure 2

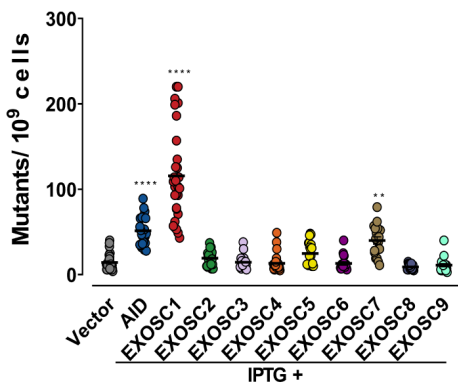
**A**



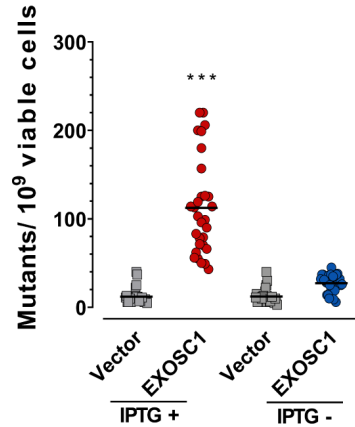
**B**



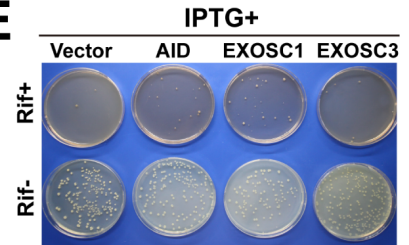
**C**



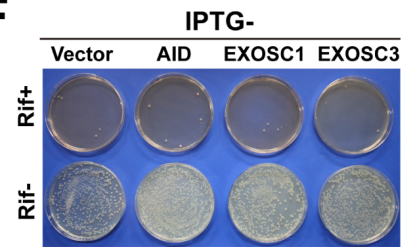
**D**



**E**



**F**



**G**

**Vector**

1521 → `ctg tct cag ttt atg gac cag aac aac ccg ctg tct gag att acg cac aaa cgt cgt atc tcc gca ctc ggc cca ggc ggt ctg acc cgt gaa cgt gca`  
`ggc ttc gaa gtt cga gac gta cac ccg act cac tac ggt cgc gta tgt cca atc gaa acc cct gaa ggt ccg aac atc ggt ctg atc aac tct ctg`  
 1725

**EXOSC1**

1521 → `ctg tct cag ttt atg gac cag aac aac ccg ctg tct gag att acg cac aaa cgt cgt atc tcc gca ctc ggc cca ggc ggt ctg acc cgt gaa cgt gca`  
`ggc ttc gaa gtt cga gac gta cac ccg act cac tac ggt cgc gta tgt cca atc gaa acc cct gaa ggt ccg aac atc ggt ctg atc aac tct ctg`  
 1725

**H**

**Vector**

		To			
		A	G	C	T
From	A		4	2	2
	G	1			2
	C		1		12
	T	2	2	4	

**I**

**EXOSC1**

		To			
		A	G	C	T
From	A			1	2
	G			1	6
	C	19	2		4
	T	1			

**J**

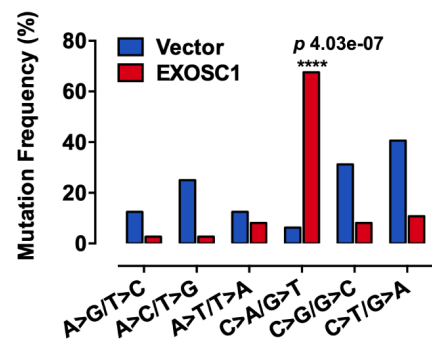
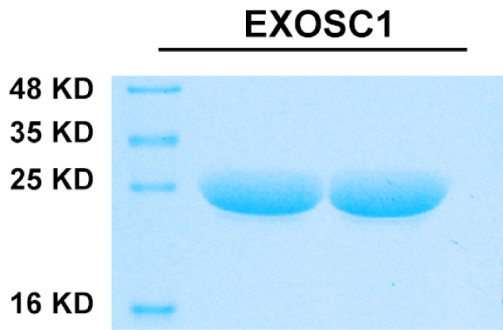
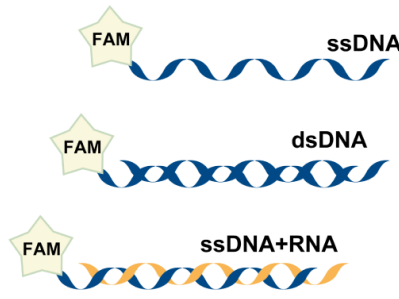


# Figure 3

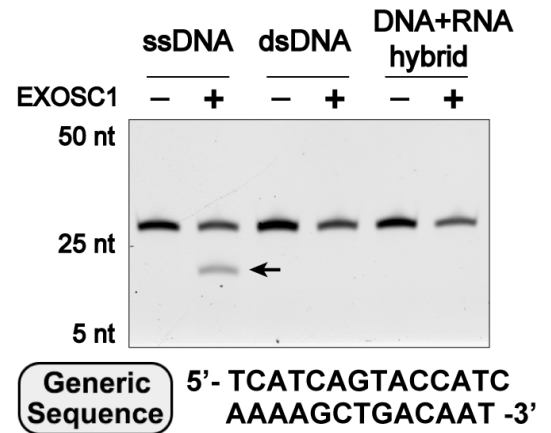
**A**



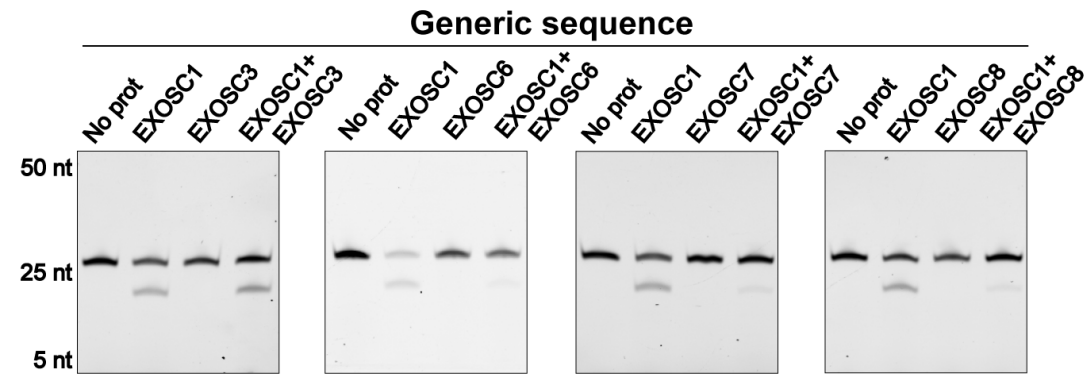
**B**



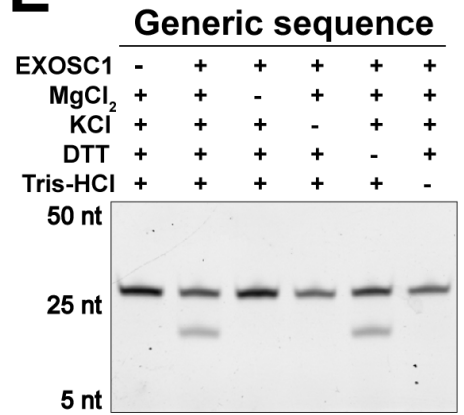
**C**



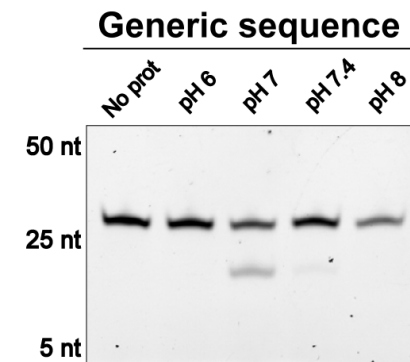
**D**



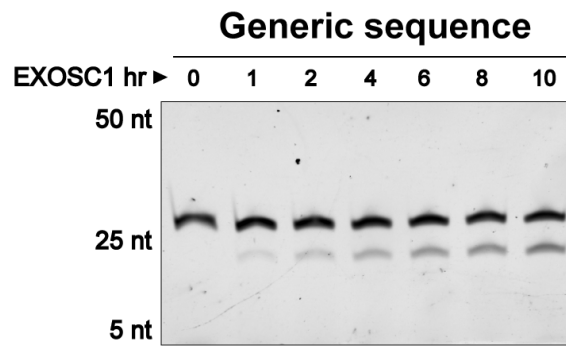
**E**



**F**



**G**



**H**

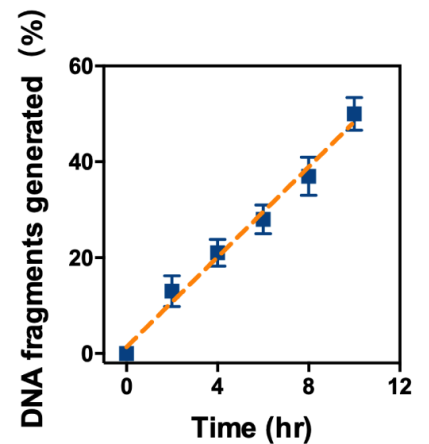
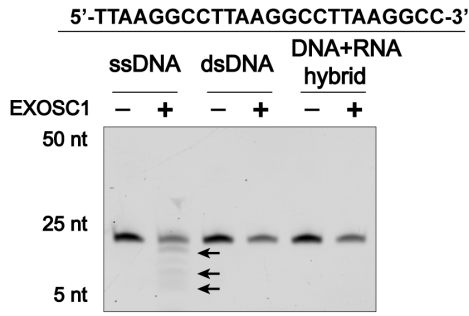
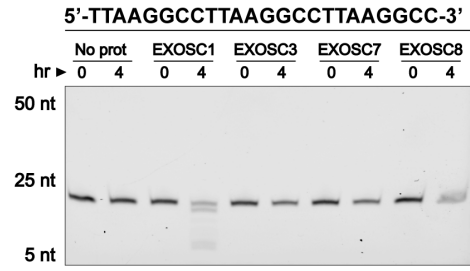


# Figure 4

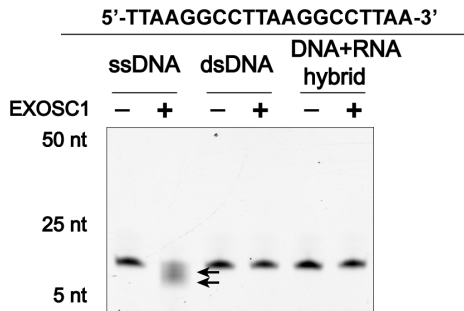
**A**



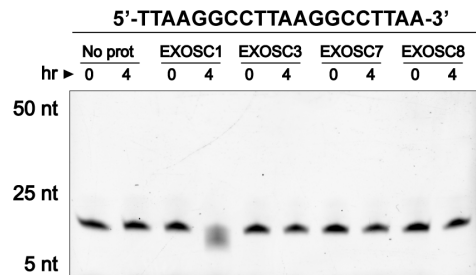
**B**



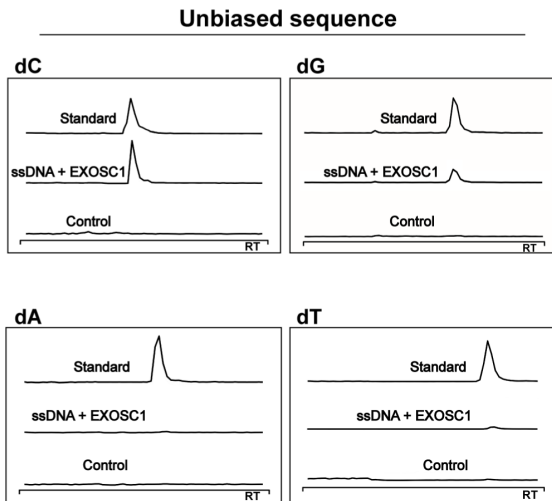
**C**



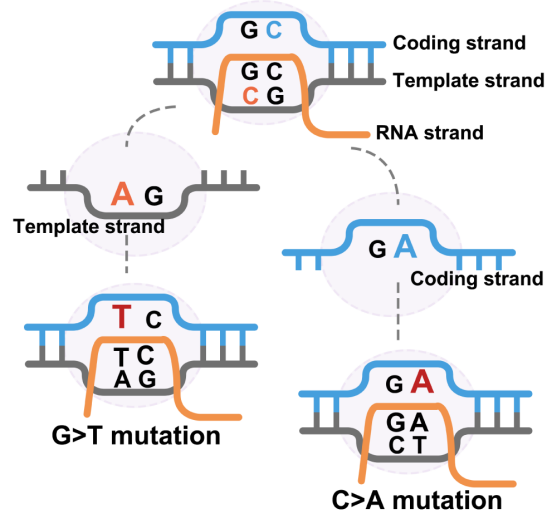
**D**



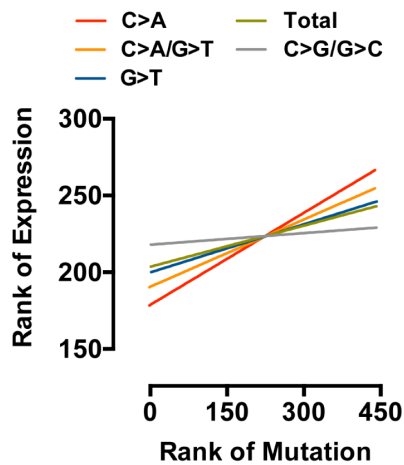
**E**



**F**



**G**



**H**

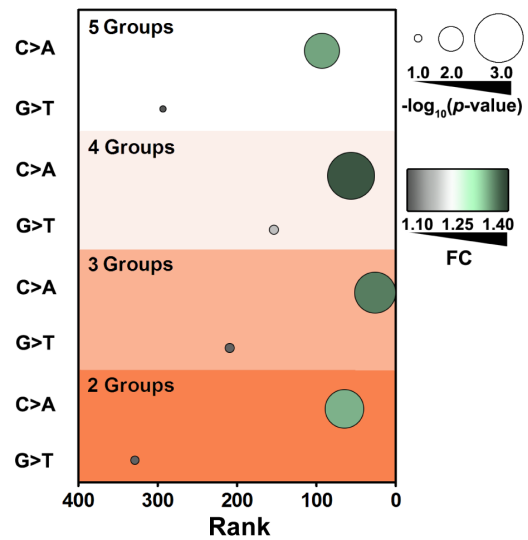


# Figure 5

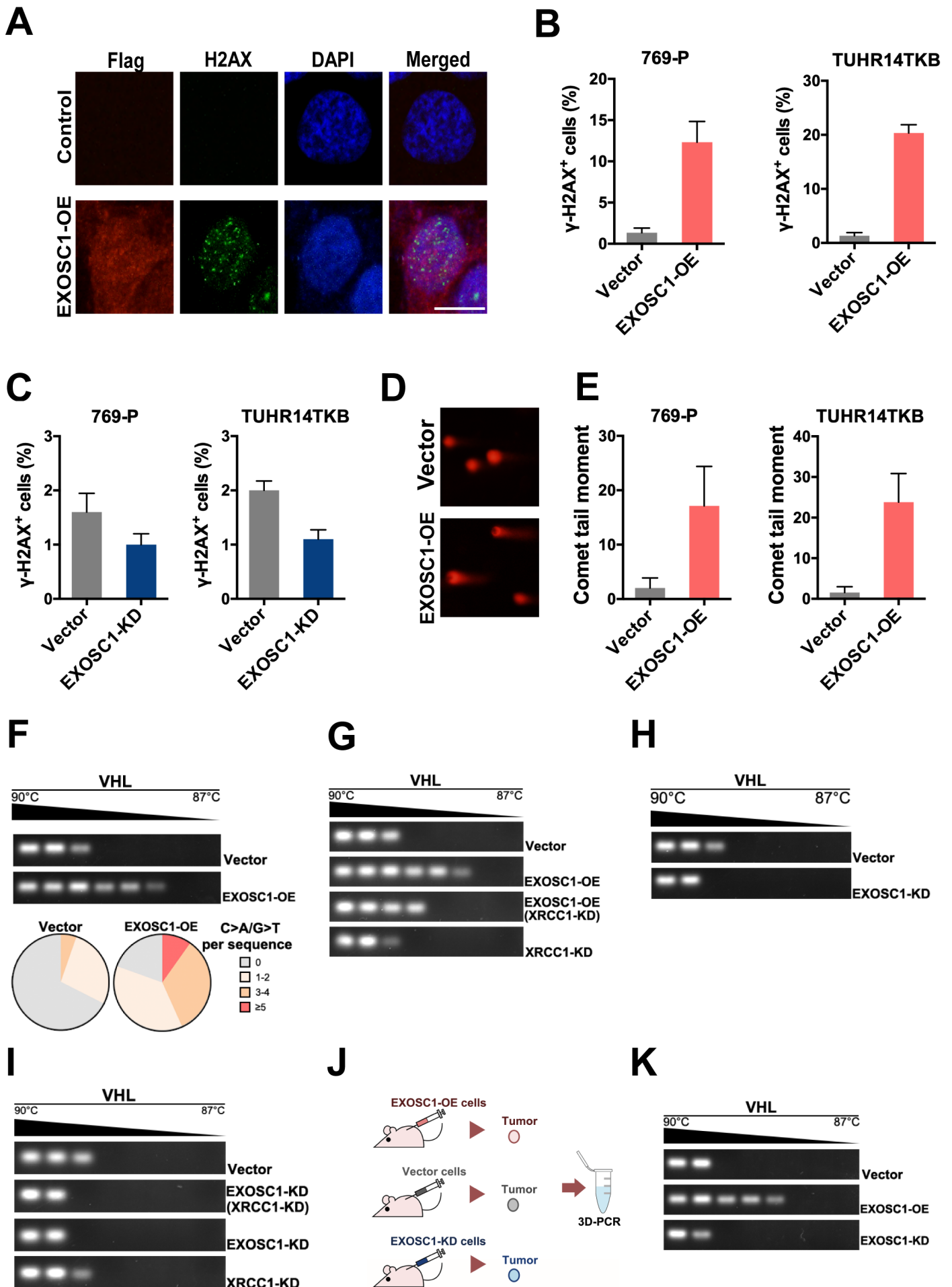
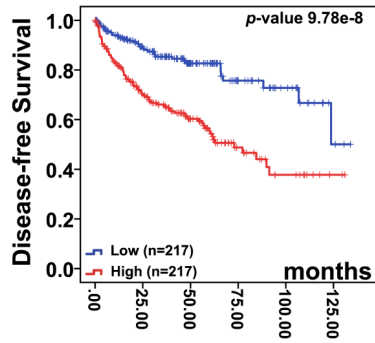
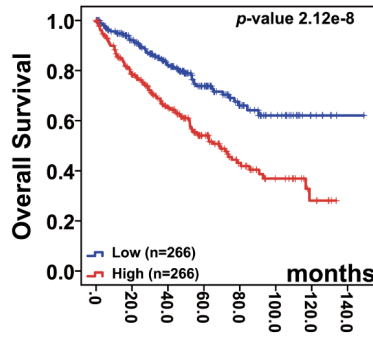


# Figure 6

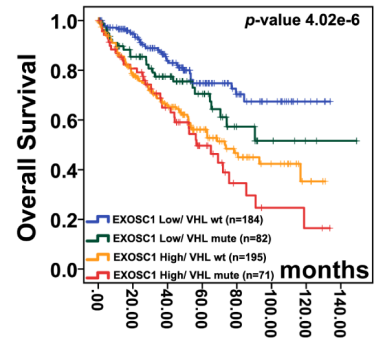
**A**



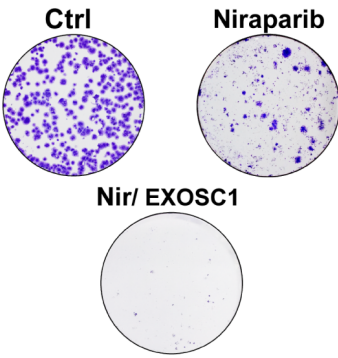
**B**



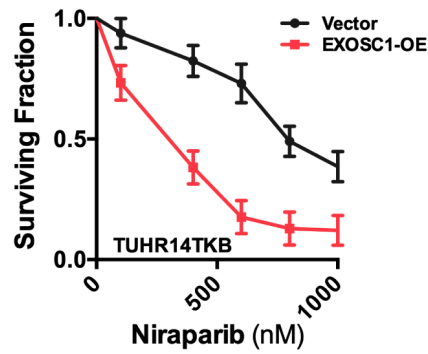
**C**



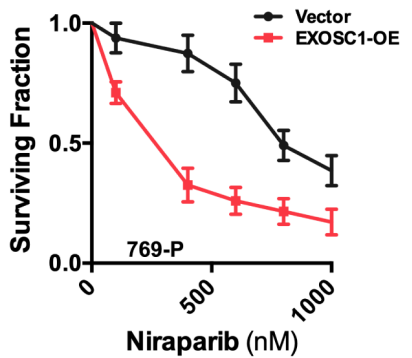
**D**



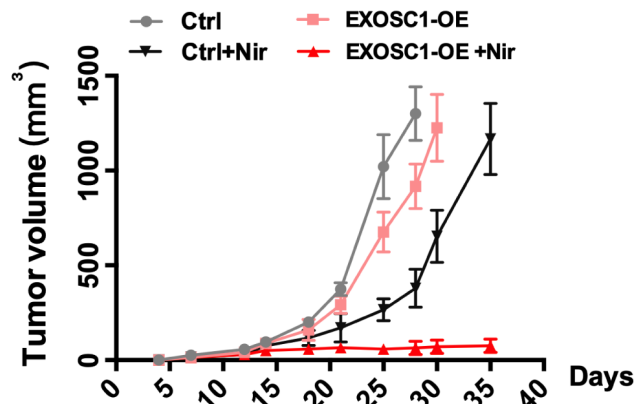
**E**



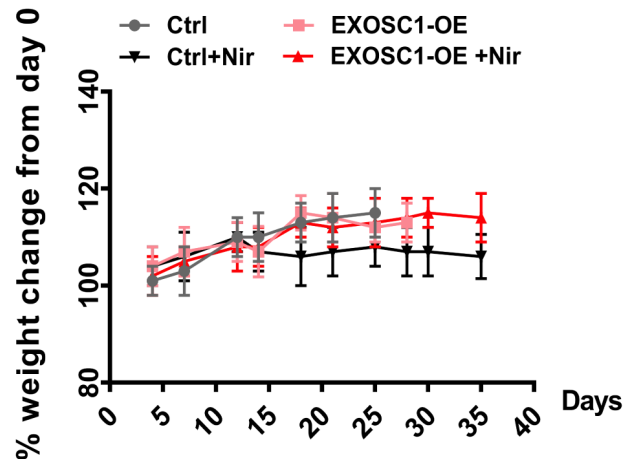
**F**



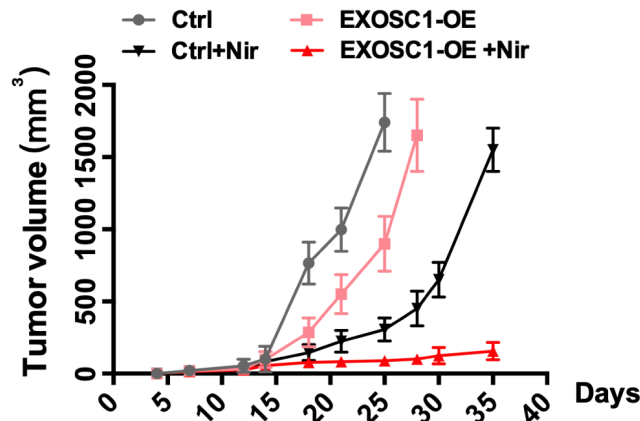
**G**



**H**



**I**



**J**

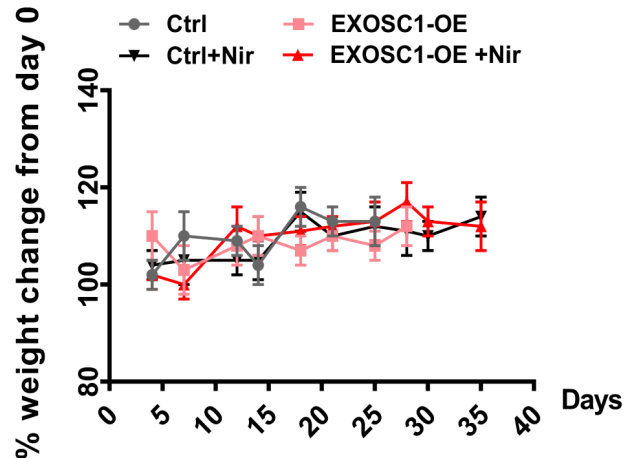
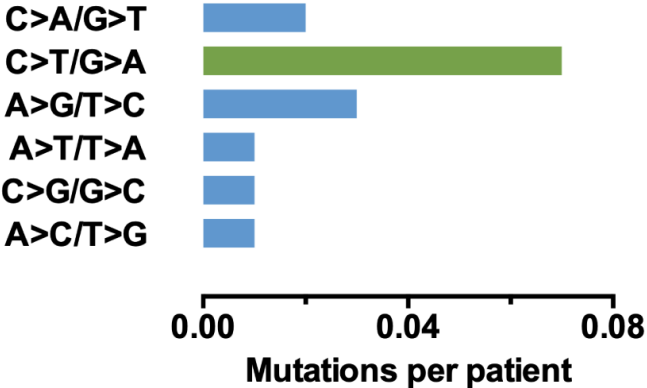




# Figure 1—figure supplement 1

**A**

**TP53 in BRCA**



**B**

**VHL in KIRC**

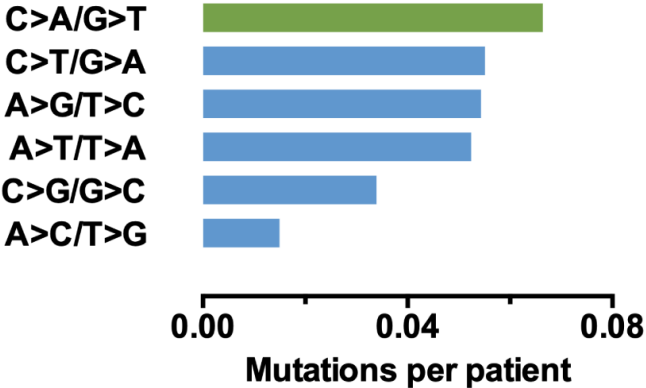
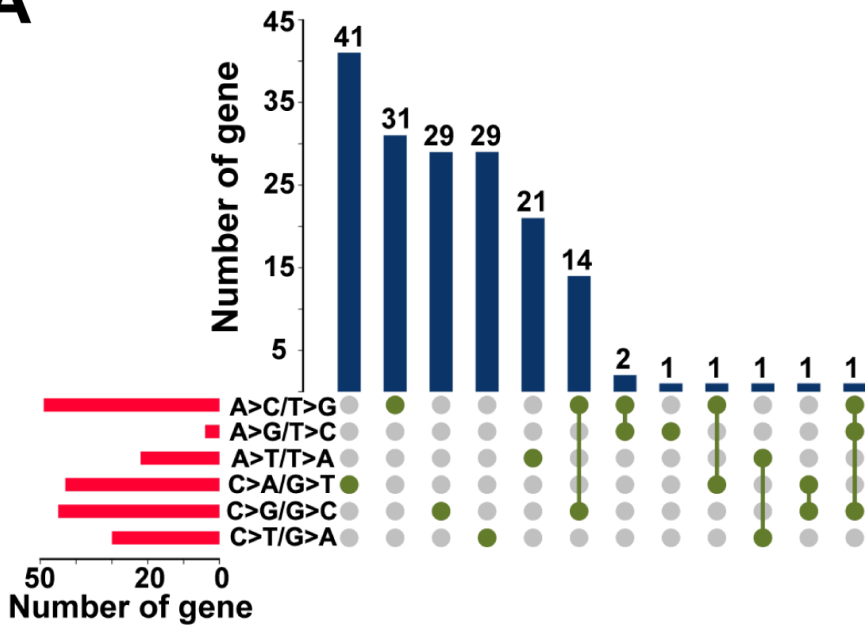
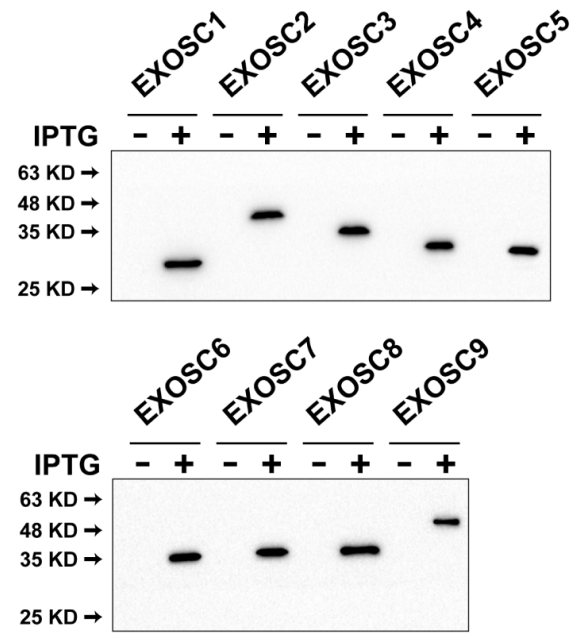


# Figure 2—figure supplement 1

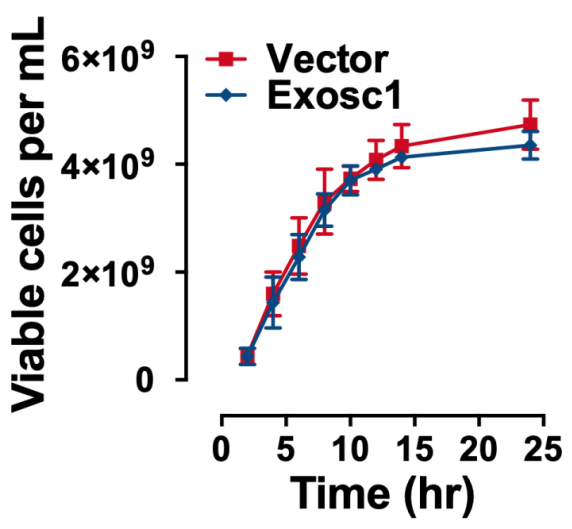
**A**



**B**



**C**



**D**

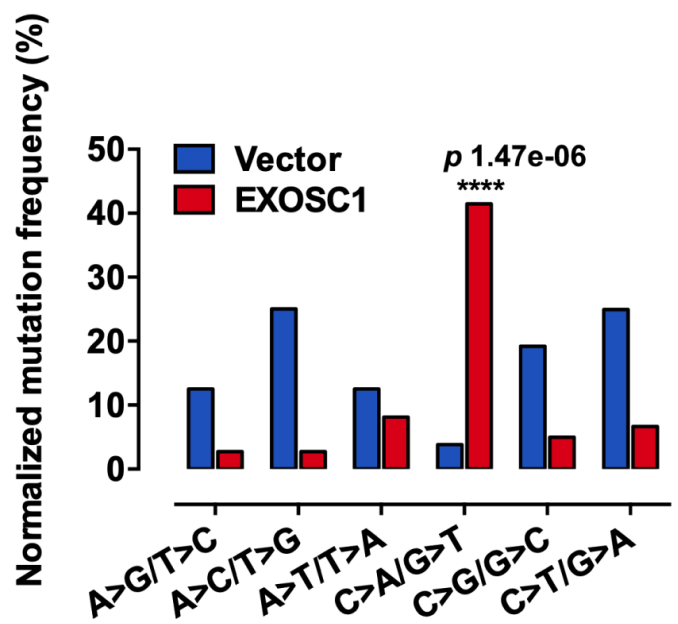
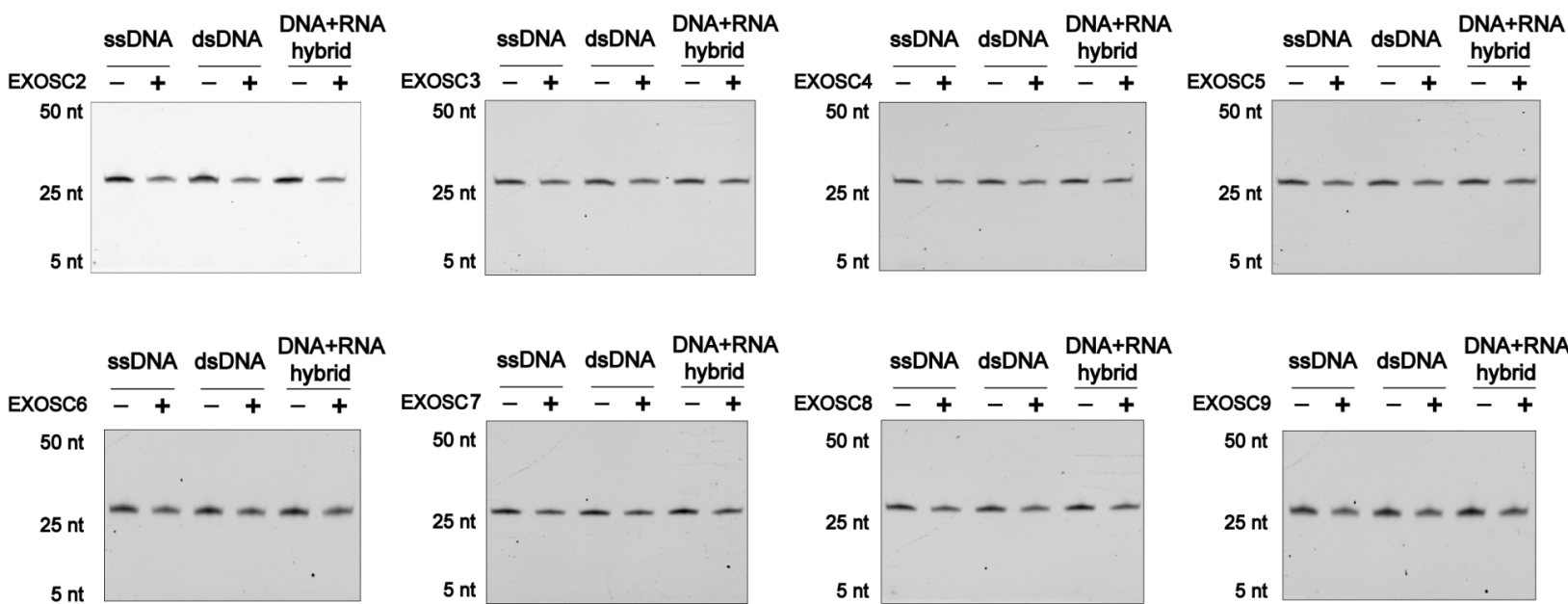


# Figure 3—figure supplement 1

**A**



**B**

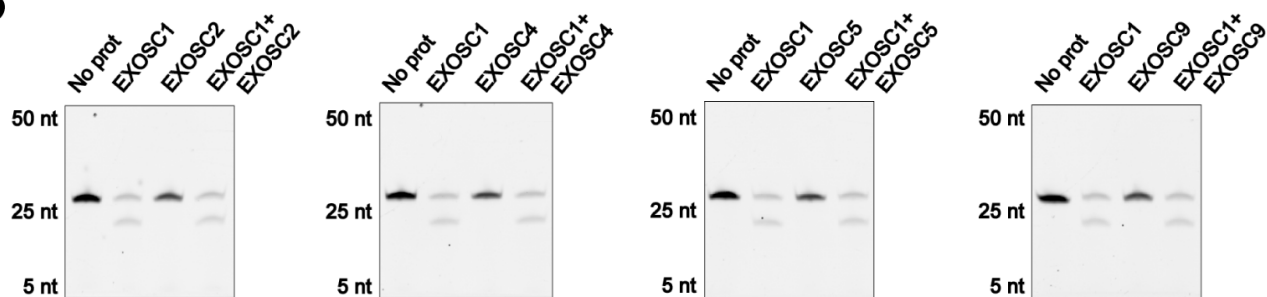
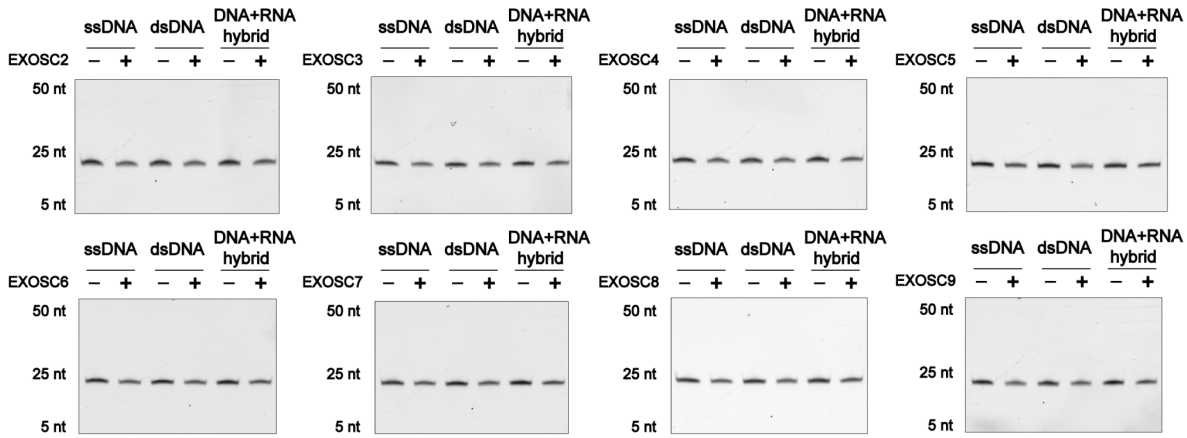
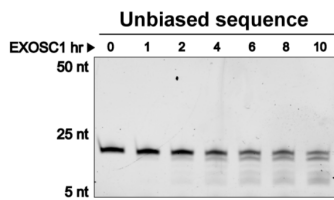


# Figure 4—figure supplement 1

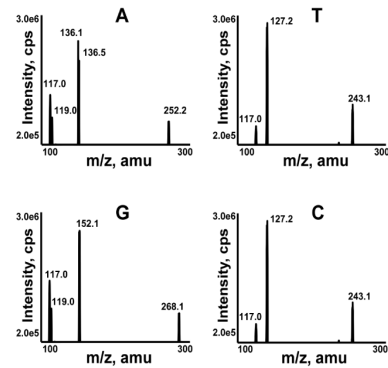
## A



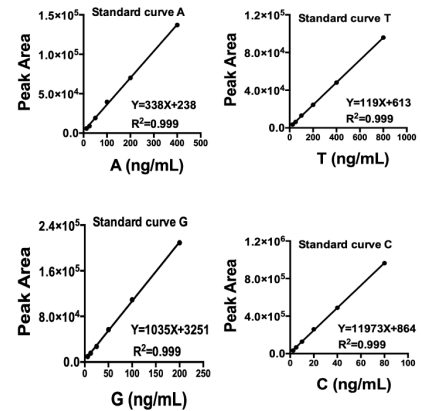
## B



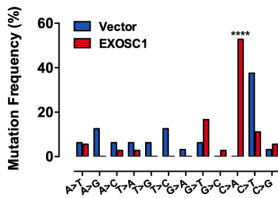
## C



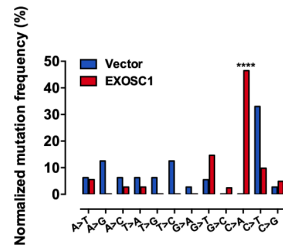
## D



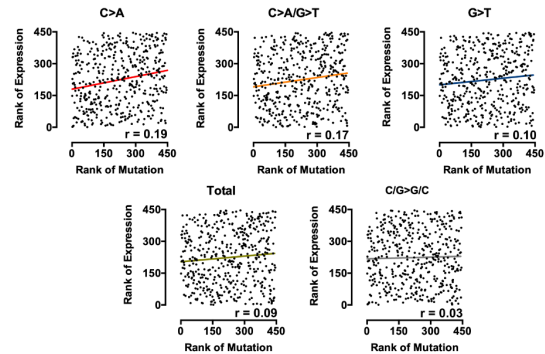
## E



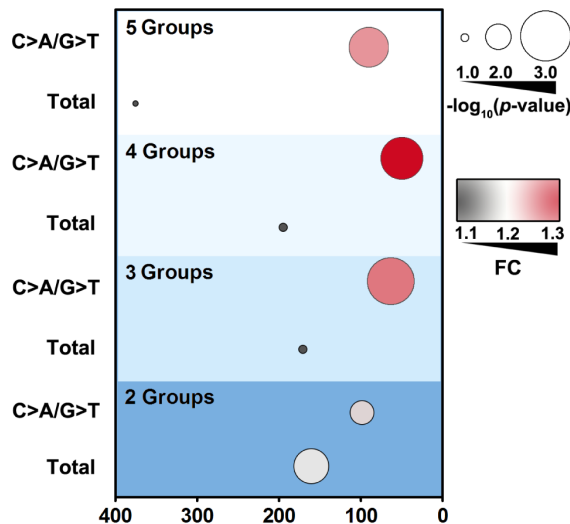
## F



## G



## H



## I

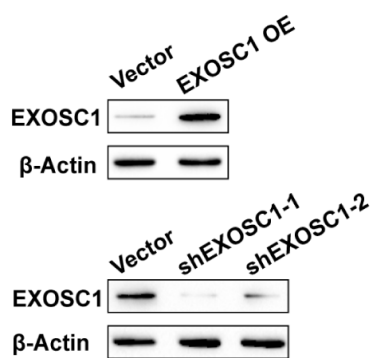
P value	C>A/G>T	Total
2-groups	0.0340	0.0078
3-groups	0.0004	0.0186
4-groups	0.0008	0.0419
5-groups	0.0054	0.1553

## J

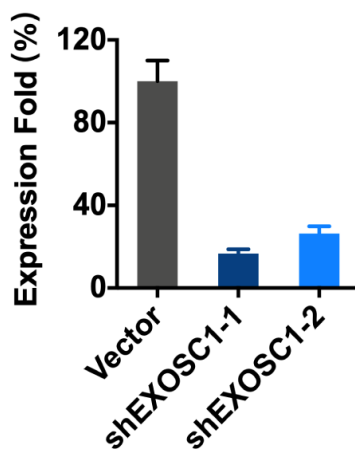
P value	C>A	G>T
2-groups	0.0001	0.0510
3-groups	0.0001	0.0210
4-groups	0.0001	0.0226
5-groups	0.0008	0.0437

# Figure 5—figure supplement 1

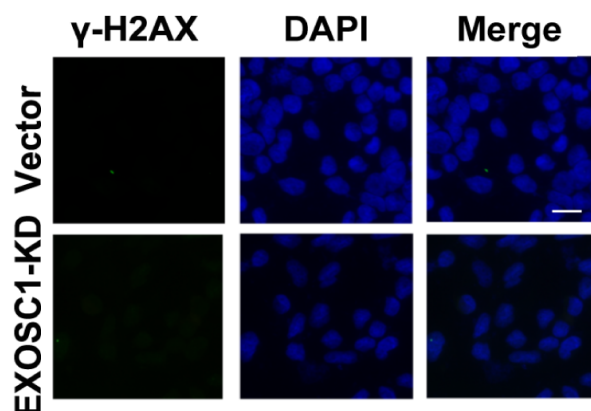
**A**



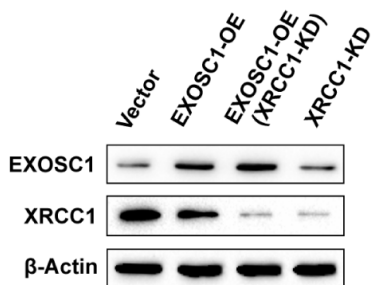
**B**



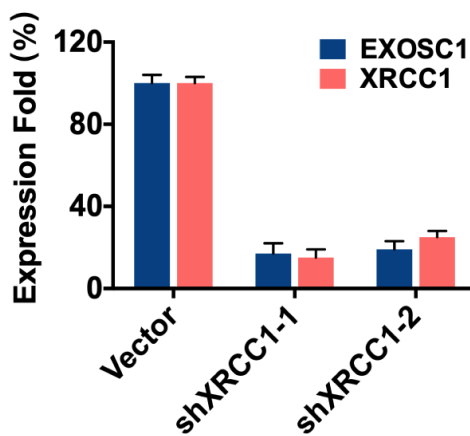
**C**



**D**



**E**



**F**

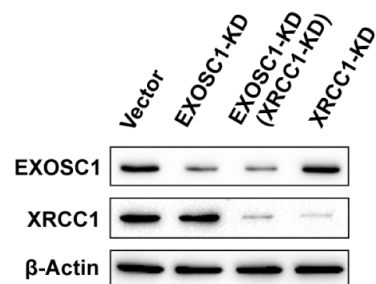
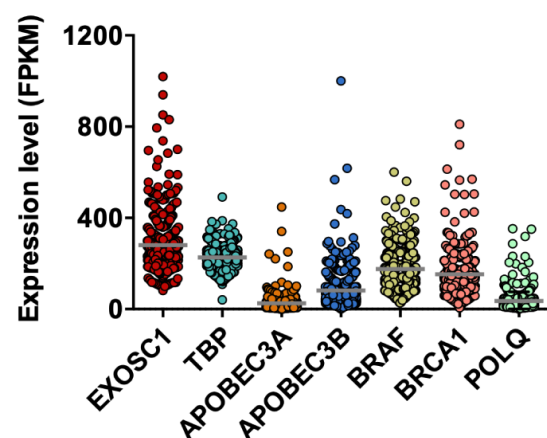
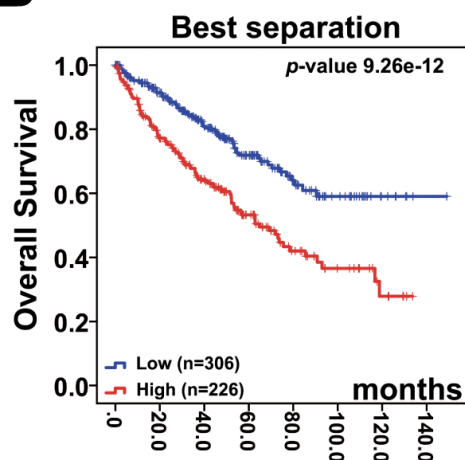


# Figure 6—figure supplement 1

**A**



**B**



**C**

	EXOSC1- VHL wt	EXOSC1- VHL mut	EXOSC1+ VHL wt	EXOSC1+ VHL mut
Median Survival (Month)	104.47	98.46	75.66	65.19
Logrank Test P-Value	4.02e-6			

**D**

